

Near–Infrared Imaging of Early–Type Galaxies III. The Near–Infrared Fundamental Plane

Michael A. Pahre^{1,2,3,4}, S. G. Djorgovski¹, and Reinaldo R. de Carvalho^{1,5}

ABSTRACT

Near–infrared imaging data on 251 early–type galaxies in clusters and groups are used to construct the near–infrared Fundamental Plane (FP)

$$r_{\text{eff}} \propto \sigma_0^{1.53 \pm 0.08} \langle \Sigma_K \rangle_{\text{eff}}^{-0.79 \pm 0.03}.$$

The slope of the FP therefore departs from the virial expectation of $r_{\text{eff}} \propto \sigma_0^2 \langle \Sigma \rangle_{\text{eff}}^{-1}$ at all optical and near–infrared wavelengths, which could be a result of the variation of M/L along the elliptical galaxy sequence, or a systematic breakdown of homology among the family of elliptical galaxies. The slope of the near–infrared FP excludes metallicity variations as the sole cause of the slope of the FP. Age effects, dynamical deviations from a homology, or any combination of these (with or without metallicity), however, are not excluded. The scatter of both the near–infrared and optical FP are nearly identical and substantially larger than the observational uncertainties, demonstrating small but significant intrinsic cosmological scatter for the FP at all wavelengths. The lack of a correlation of the residuals of the near–infrared FP and the residuals from the $\text{Mg}_2\text{--}\sigma_0$ relation indicates that the thickness of these relations cannot be ascribed only to age or metallicity effects. Due to this metallicity independence, the small scatter of the near–infrared FP excludes a model in which age and metallicity effects “conspire” to keep the optical FP thin. All of these results suggest that the possible physical origins of the FP relations are complicated due to combined effects of variations of stellar populations and structural parameters among elliptical galaxies.

Subject headings: galaxies: elliptical and lenticular, cD — galaxies: photometry — galaxies: fundamental parameters — galaxies: stellar content — infrared: galaxies

¹Palomar Observatory, California Institute of Technology, MS 105-24, Pasadena, CA 91125; *email:* george@astro.caltech.edu .

²Guest Observer, Las Campanas Observatory.

³Present address: Harvard-Smithsonian Center for Astrophysics, 60 Garden Street, MS 20, Cambridge, MA 02138; *email:* mpahre@cfa.harvard.edu .

⁴Hubble Fellow.

⁵Departamento de Astrofísica, Observatorio Nacional, CNPq, Brazil; *email:* reinaldo@maxwell.on.br .

1. Introduction

Correlations among the properties of elliptical galaxies have been used both as measures of their homogeneity as a population and as indicators of the distances of individual galaxies. The discovery of a color–magnitude effect (Baum 1959) was followed by the measurement of relative distances of galaxies and clusters using the color–magnitude relation (Sandage 1972; Visvanathan & Sandage 1977; Sandage & Visvanathan 1978a,b). The relation’s small scatter was used as a constraint on elliptical galaxy formation time-scales (Bower, Lucey, & Ellis 1992). The correlation between luminosity and velocity dispersion (Faber & Jackson 1976) was likewise used as a distance indicator (Tonry & Davis 1981; Dressler 1984), but Terlevich *et al.* (1981) discovered a weak correlation between the residuals of the relation and Mg_2 , implying that there might be a second parameter which contributes to the intrinsic scatter of the Faber–Jackson relation.⁶ Subsequent studies (Dressler *et al.* 1987; Djorgovski & Davis 1987) that included large samples of elliptical galaxies found that surface brightness was a second parameter which caused a large portion of the scatter in the Faber–Jackson relation. In this perspective, the intrinsic properties of elliptical galaxies are only found to lie on a plane within the three–dimensional parameter space of the observables. This Fundamental Plane (FP) is thus a set of bivariate correlations between the observed properties of elliptical galaxies; the color–magnitude and Faber–Jackson relations are projections of that plane onto two of the three axes.

The importance of the exact form of the slope of the FP was immediately identified as possibly providing a strong constraint on the mass–to–light ratios (M/L) of elliptical galaxies (Dressler *et al.* 1987; Djorgovski & Davis 1987). In particular, the virial theorem produces a prediction that $r_{\text{eff}} \propto \sigma_0^2 \langle \Sigma \rangle_{\text{eff}}^{-1}$ (where r_{eff} is the effective radius, σ_0 is the central velocity dispersion, and $\langle \Sigma \rangle_{\text{eff}}$ is the mean surface brightness enclosed within r_{eff}) if two assumptions are made: (1) M/L is the same for all elliptical galaxies, and (2) elliptical galaxies form a homologous family in their scaling properties. The latter assumption was generally taken to be true, hence virtually all researchers in the last decade have proceeded to explore the effects of the variations of M/L implied by the FP correlations. For example, the slope of $D_n \propto \sigma_0^{1.2}$ from Lynden–Bell *et al.* (1988) in the B –band implies that M/L varies systematically with the galaxy’s luminosity as $M/L_B \propto L_B^{0.32}$.

More recently, there have been a variety of theoretical (Capelato, de Carvalho, & Carlberg 1995, 1997; Ciotti, Lanzoni, & Renzini 1996) and observational (Graham & Colless 1997; Busarello *et al.* 1997) investigations into the question of whether or not elliptical galaxies form a homologous scaling family. The results of these studies are not yet clear, but they seem to imply that structural deviations of the light profiles of ellipticals from a homologous family cannot affect the FP

⁶Dressler *et al.* (1987) describe how this evidence for the bivariate nature of elliptical galaxies found by Terlevich *et al.* (1981) might actually have been driven more by distance errors in the Terlevich *et al.* sample, which was drawn primarily from the field, and from a surface brightness correlation which was later found to be the second parameter. After correcting for surface brightness effects, Dressler *et al.* found little or no correlation among the residuals of the Faber–Jackson relation and Mg_2 .

appreciably (Graham & Colless 1997), while dynamical deviations from a homologous family can (Capelato *et al.* 1995; Busarello *et al.* 1997; cf. Graham & Colless 1997). Underlying all of these studies is an important point: if there are significant and systematic deviations from a homology, then these deviations should be strictly independent of wavelength observed in constructing the global photometric parameters which enter the FP.

In a broad sense, some of these possible implications of the FP make specific predictions which can be tested by obtaining additional data. For example, if the form of the FP is a direct result of a dependence of M/L on L due to variations in the stellar populations parameters of age and/or metallicity, then observations in the near-infrared should show a significantly different form for the FP correlations as the $2.2\mu\text{m}$ light is far less sensitive than optical light to line-blanketing and somewhat less sensitive to age effects. Alternatively, if the origin of the FP is due to a systematic deviation of elliptical galaxies from a homologous family, then the exact form of the FP should be independent of wavelength. It is also possible that some combination of these effects could be required by a simultaneous analysis of the FP at optical and near-infrared wavelengths.

The present paper is an attempt to address these possible origins for the FP correlations by exploring their form using near-infrared imaging data. Early work on the FP in the K -band was done by Recillas-Cruz *et al.* (1990, 1991), who obtained aperture photometry for galaxies in Virgo and Coma, and Djorgovski & Santiago (1993), who used aperture photometry from Persson, Frogel, & Aaronson (1979). Both studies relied on optical estimates of r_{eff} . It follows directly from the existence of color gradients that r_{eff} should be smaller for longer wavelengths and this point will be shown explicitly in a future paper (Pahre, de Carvalho, & Djorgovski 1998) for these optical and near-infrared data. The present paper is more than just a revisiting of the K -band FP—it is an attempt to study the global properties of elliptical galaxies using near-infrared photometry that is fully independent of the optical photometry, while at the same time using a methodology for deriving global photometric parameters that is identical to the method at optical wavelengths.

An imaging survey of this kind and scale has only recently become possible with the introduction of large format IR detectors (256×256 pixel²). This project was initiated during the commissioning phase of a wide-field, near-infrared imaging camera (Murphy *et al.* 1995) for the Palomar 60-inch Telescope. In the first paper of this series, early results from this survey on the K -band FP (Pahre, Djorgovski, & de Carvalho 1995) indicated that there is a modest change in slope from the optical to the near-infrared, but not nearly as much variation as would be expected if stellar-populations alone were the cause of the slope of the FP (Pahre & Djorgovski 1997; Pahre, Djorgovski, & de Carvalho 1997). The full K -band survey and the complete catalogs of global properties are described in the second paper of this series (Pahre 1998) and are summarized in §2. All of the data contained in the previous contributions (Pahre *et al.* 1995, 1997; Pahre & Djorgovski 1997) were re-calibrated, some were re-reduced, and the global photometric parameters re-derived in a consistent manner as described in Pahre (1998). The FP correlations and their many projections are derived in §3 as a way of exploring various aspects of these near-infrared data. The $\text{Mg}_2\text{-}\sigma_0$ relation is constructed for the same galaxies in §3.4. Simple models will be

compared to these results in §4, but it will be shown that naive models cannot explain the many observed properties of ellipticals nor are such models unique.

2. Description of the Data

The data used for this paper derive from Pahre (1998). That paper presented near-infrared K -band imaging of 341 early-type galaxies, and used those data to measure the global photometric parameters of the half-light effective radius r_{eff} , the mean surface brightness $\langle\mu\rangle_{\text{eff}}$ enclosed by that radius, the total magnitude K_{tot} , and the diameter D_K at which the mean surface brightness, fully corrected for cosmological effects and extinction, drops to 16.6 mag arcsec⁻². The latter quantity is an analog of the B -band D_n parameter defined by Dressler *et al.* (1987). The near-infrared data were corrected for the effects of seeing. As shown in that paper, the random uncertainties of the measured quantities are: 0.06 dex on r_{eff} ; 0.21 mag on $\langle\mu\rangle_{\text{eff}}$; 0.09 mag on K_{tot} ; 0.010 dex on D_K ; and 0.015 dex on $r_{\text{eff}} - 0.32\langle\mu\rangle_{\text{eff}}$, the quantity which will enter the FP.

The galaxies in that sample are primarily drawn from nearby rich clusters of galaxies, although additional galaxies were added from groups and the general field. The galaxies were not selected according to any explicit criteria of completeness (such as a magnitude-limited sample would be), but by the availability of companion optical imaging and spectroscopic data. The primary goal of this effort was to provide a large sample of galaxies for which the variations of the FP correlations between the optical and near-infrared wavelengths could be explored. The data probe the full range of properties (r_{eff} , K_{tot} , σ_0) displayed by the family of giant elliptical galaxies, and a significant portion of the sample is comprised of S0 galaxies.

The optical global photometric parameters (r_{eff} , $\langle\mu\rangle_{\text{eff}}$, and D_n) and spectroscopic parameters (central velocity dispersion σ_0 and Magnesium line index Mg_2) were compiled from the literature by Pahre (1998). All of the photometry were drawn from the U , B , g , V , R_C (or r), or I_C bandpasses and converted to V magnitudes for a general catalog. Furthermore, separate catalogs were constructed for individual comparisons to preserve the wavelength information for each optical bandpass. The spectroscopic parameters were corrected for observed aperture size effects to a common physical scale of $1.53h_{75}^{-1}$ kpc; small offsets between data sets have been applied according to prescriptions developed by other authors in the literature. The values were then averaged to reduce the random uncertainties and minimize systematic errors due to some data sets. Of the 341 galaxies imaged in the K -band, 95% have velocity dispersions, 69% have Mg_2 indices, and 91% have optical photometric parameters (either r_{eff} or D_n). The typical uncertainties for individual measurements of σ_0 and Mg_2 are 0.04 dex and 0.013 mag (Smith *et al.* 1997), respectively. A substantial fraction of the entire sample has more than one measurement of these parameters which were then averaged, so these two uncertainty estimates can be taken as a universal upper limit to the measurement uncertainties.

Many, if not most, of the literature sources suggest that their velocity dispersions are less

reliable below 100 km s^{-1} , but a bias in the slope of the FP can be introduced by imposing a cut on σ_0 . It will be important to investigate what effect changing the lower cutoff for σ_0 has on the slope and scatter of the FP. Small measures of the effective radius, such as $r_{\text{eff}} \leq 1 \text{ arcsec}$ (the median seeing was 1.34 arcsec FWHM), have large random uncertainties and probably substantial systematic errors, and should probably also be discarded. In the sample, 4% of the galaxies have morphological type SB0 or later, and another 4% have S0/a type; caution should be exercised when studying the global properties of these galaxies. One galaxy (D45 in cluster Abell 194) appears to be a misidentification either in the optical or near-infrared as evidenced by its color $(V - K) = 1.28 \text{ mag}$, which appears to be much too blue compared to the mean $(V - K) = 3.15 \text{ mag}$ for the entire sample. Five galaxies in the Virgo cluster were removed from the sample, as their accurate distances as derived by the surface brightness fluctuations method (provided by J. Blakeslee and J. Tonry; see Tonry *et al.* 1997) show that they are either in the background W Cloud (NGC 4168, NGC 4261, and NGC 4365) or the foreground (NGC 4660 and NGC 4697).

3. Analysis of the Elliptical Galaxy Correlations

3.1. The Near-Infrared Fundamental Plane

Galaxies were drawn from the sample described in §2. Only those galaxies residing in a cluster or group with four or more observed galaxies were included in the FP fits, resulting in 16 clusters/groups and 249 galaxies with $\sigma_0 > 1.8$. Two of the five Leo I Group galaxies were excluded as a result of these selection criteria, although the remaining three galaxies were retained in the sample for completeness.

The “standard” FP equation is usually written as

$$\log r_{\text{eff}}(\text{arcsec}) = a \log \sigma_0(\text{km s}^{-1}) + b \langle \mu \rangle_{\text{eff}}(\text{mag arcsec}^{-2}) + c_i \quad (1)$$

where a is usually identified as the “slope” of the FP and c_i are the “intercepts.” The intercept of the relation will vary with distance. The galaxies in each of the 16 groups and clusters are assumed to lie at the same distance, hence there are $i = 16$ different intercepts c_i .

The Equation 1 was fit by minimizing the sum of the absolute deviations of the points orthogonally from the relation using the program GAUSSFIT (Jefferys *et al.* 1987). During the first iteration, two points which are outliers (D9 in Cen30 and S201 in Hydra) were identified and excluded from the analysis. The resulting FP in the near-infrared K -band is

$$\log r_{\text{eff}}(\text{arcsec}) = \begin{array}{l} 1.53 \log \sigma_0 + \quad 0.314 \langle \mu_K \rangle_{\text{eff}} + c_i \quad N = 251 \quad \text{rms} = 0.096 \text{ dex} \\ \pm 0.08 \quad \quad \quad \pm 0.011 \end{array} \quad (2)$$

The uncertainties in the coefficients were determined by 100 iterations of bootstrap resampling of the data-points. The individual intercepts c_i for the fit, and the rms about the fit for each cluster

or group, are listed in Table 1. Since the rms is quoted in units of $\log r_{\text{eff}}$, the uncertainty on each intercept is therefore $\text{rms}/\sqrt{N-1}$. The relation in Equation 2 is equivalent to the scaling relation $r_{\text{eff}} \propto \sigma_0^{1.53 \pm 0.08} \langle \Sigma_K \rangle_{\text{eff}}^{-0.79 \pm 0.03}$.

Changing the lower cutoff for σ_0 from 1.8 dex to 2.0 dex changes the value of a by ≤ 0.01 dex, changes b by ≤ 0.001 dex, reduces the scatter by 10% to 0.089 dex, and excludes 23 galaxies (9% of the total). Hence, the solution to the FP is robust to the lower σ_0 cutoff, although the galaxies with the lowest σ_0 appear to contribute the largest to the observed scatter. Minimizing the orthogonal variance (instead of the absolute value of the deviation) from the FP relation with $\sigma_0 \geq 1.8$ dex results in a small change in the slope of the FP to:

$$\log r_{\text{eff}}(\text{arcsec}) = \begin{array}{l} 1.63 \log \sigma_0 + 0.320 \langle \mu_K \rangle_{\text{eff}} + c_i \\ \pm 0.06 \qquad \qquad \pm 0.008 \end{array} \quad N = 251 \quad \text{rms} = 0.099 \text{ dex} \quad (3)$$

Since the coefficients in Equations 2 and 3 are equivalent within the uncertainties, the fit to the FP is insensitive to the exact fitting method. The method of minimizing the absolute value of the orthogonal deviation from the fit is to be preferred, however, as it is less sensitive to outliers.

The simultaneous fit to all clusters is displayed in Figure 1 with the data subdivided into the 16 individual clusters or groups. It is clear from this figure that the simultaneous fit is a representative description of the properties of the early-type galaxies in all of the clusters. There is no clear deviation from this mean relation.

The 11 clusters with more than ten galaxies were fit individually to Equation 1 as a test of the universality of the FP relation. The difficulty with all 11 separate fits, however, is that the number of galaxies in each cluster is small enough that the slope of the relation is not accurately determined. Once again, the uncertainties on the fitted coefficients a and b have been determined using the bootstrap procedure. In eight of the 11 cases, the fits have a within one standard deviation of the value $a = 1.53$ from the simultaneous fit, suggesting both that the uncertainties are reasonably estimated and that better fits are limited by the number of galaxies per cluster. These individual fits are listed in Table 1.

The same 11 clusters were also fit individually by constraining $b = 0.314$ from the previous simultaneous fit. This is possible because virtually every study of the FP (optical and near-infrared) obtains a similar value for this parameter, hence it should be possible to constrain its value *a priori*. These fits show significantly smaller uncertainty in their determination of a than the unconstrained fits, and are listed in Table 1. In this case, seven of the 11 clusters have a slope a within one standard deviation of the value from the simultaneous fit.

The adopted form of the FP in Equation 2 is plotted for all 301 galaxies in these 16 clusters and groups in Figure 2, both in face-on and edge-on perspectives. While the edge-on view with $\log R_{\text{eff}}$ as the ordinate⁷ is the most common method of displaying the FP, the edge-on view

⁷In this paper, a distinction will be made between the angular effective radius r_{eff} , measured in arcsec, and the

with $\log R_{\text{eff}} - 0.314\langle\mu\rangle_{\text{eff}}$ as the ordinate is easier to interpret. Virtually every study of the FP (optical and near-infrared) obtains the same relationship between R_{eff} and $\langle\mu\rangle_{\text{eff}}$, but there may be significant variation in the relationship between $(\log R_{\text{eff}} - 0.314\langle\mu\rangle_{\text{eff}})$ and $\log \sigma_0$, depending on wavelength. Furthermore, this edge-on perspective of the FP, seen from its short side, separates the correlated measurement errors in r_{eff} and $\langle\mu\rangle_{\text{eff}}$ from the independent measurement errors in σ_0 . The FP in physical units as plotted in Figure 2 is $\log R_{\text{eff}}(h_{75}^{-1} \text{ kpc}) = 1.53 \log \sigma_0 + 0.314\langle\mu\rangle_{\text{eff}} - 8.30$.

In the face-on view of the FP in Figure 2(c), it is seen that galaxies do not uniformly populate this planar surface. While the K -band data in this paper are not drawn from a strictly magnitude-limited sample, they do behave as though a $K_{\text{tot}} \lesssim 13$ mag limit were imposed. Most of the galaxies are found to have $15 < \langle\mu_K\rangle_{\text{eff}} < 18$ mag arcsec $^{-2}$ (long-dashed lines), although there are no clear selection effects causing this distribution of galaxy properties. Furthermore, there are no galaxies with properties in the upper-right portion of the figure, which could be caused by the lack of galaxies with central velocity dispersions $\sigma_0 > 400$ km s $^{-1}$, although there is no selection limit imposed on this portion of the FP.

3.2. The D_K - σ_0 Relation

Dressler *et al.* (1987) introduced a parameter D_n which was defined as the diameter at which the circular mean surface brightness (fully corrected for cosmological effects and Galactic extinction) dropped to a fiducial value. This parameter was chosen, in effect, to be a combination of the r_{eff} and $\langle\mu\rangle_{\text{eff}}$ terms in the FP correlations, thereby simplifying the FP to a D_n - σ_0 relation. They defined this fiducial surface brightness to be 20.75 mag arcsec $^{-2}$ in the B -band: the surface brightness was faint enough that D_B was typically much larger than the seeing disk, while bright enough that interpolation (rather than extrapolation) was used to evaluate D_B from their aperture magnitude data.⁸

Lucey & Carter (1988) defined an equivalent D_V parameter in the V -band to be the diameter at which the mean surface brightness drops to 19.8 mag arcsec $^{-2}$ (this assumes a mean galaxy color of $(B - V)_0 = 0.95$ mag), Smith *et al.* (1997) defined D_R for the R_C -band to be at $\langle\mu\rangle_{\text{eff}} = 19.23$ mag arcsec $^{-2}$ (assuming $(V - R_C) = 0.57$ mag), Jørgensen *et al.* (1995a) defined the Gunn r -band $D_r \equiv 2r_n$ to be at $\langle\mu\rangle_{\text{eff}} = 19.6$ mag arcsec $^{-2}$ (assuming $(V - r) = 0.2$ mag), and Pahre (1998) defined the K -band D_K to be at $\langle\mu\rangle_{\text{eff}} = 16.6$ mag arcsec $^{-2}$ (assuming $(V - K) = 3.2$ mag). By using typical colors for early-type galaxies in constructing these definitions, the average value of D measured for a sample of galaxies should be approximately

effective radius R_{eff} in physical scale, measured in kpc.

⁸The notation of D_B will be adopted for the rest of the paper to distinguish the D_n parameter as defined in the B -band from the equivalent diameter as defined in another bandpass. The name “ D - σ_0 relation” will refer to the correlation in all bandpasses.

independent of bandpass. The slope of the D – σ_0 relation may vary between bandpasses, however, causing there to be a systematic variation of the D parameter as a *function of σ* in different bandpasses (while keeping the mean D similar). For example, if $D_V \propto \sigma^{a_V}$ and $D_K \propto \sigma^{a_K}$, then $\log D_V - \log D_K = (a_V - a_K) \log \sigma + \text{constant}$.

The D_K – σ_0 relation was fit for the galaxies in the same 16 clusters and groups as in §3.1, excluding galaxies using similar criteria ($D_K < 2$ arcsec, $\log \sigma_0 < 1.8$, late types), and using the bootstrap method to estimate uncertainties in the fitted coefficients. The best fitting relation is

$$\log D_K (h_{75}^{-1} \text{ kpc}) = 1.62 \log \sigma_0 - 2.984 \quad N = 252 \quad \text{rms} = 0.112 \text{ dex} \pm 0.07 \quad (4)$$

and is displayed in Figure 3. The slope of this relation is consistent, given the estimated uncertainties, with the full FP relation in Equations 2 and 3. The scatter of the D_K – σ_0 relation, however, is 15% higher than the K –band FP, despite the fact that the measurement uncertainty of D_K is actually smaller than that for $r_{\text{eff}} - 0.32 \langle \mu \rangle_{\text{eff}}$ (Pahre 1998). This is most likely due to the fact that the D_K – σ_0 relation is nearly, but not quite, viewing the FP edge-on.

3.3. The FP As Seen in κ –Space

Since elliptical galaxies only populate a plane in the three-dimensional space of the observables $(R_{\text{eff}}, \langle \mu \rangle_{\text{eff}}, \sigma_0)$, it is straightforward to construct an orthogonal transformation from this observed coordinate system to another one which might facilitate a physical interpretation of the underlying parameters. Since there are many possible transformations to accomplish this, the chief practical difficulty is identifying a transformation which permits a robust and unbiased physical interpretation of the true galaxy properties (Djorgovski, de Carvalho, & Han 1988). A transformation of this kind was proposed by Bender, Burstein, & Faber (1992):

$$\begin{aligned} \kappa_1 &\equiv (2 \log \sigma_0 + \log R_{\text{eff}}) / \sqrt{2} \\ \kappa_2 &\equiv (2 \log \sigma_0 + 0.8 \langle \mu \rangle_{\text{eff}} - \log R_{\text{eff}}) / \sqrt{6} \\ \kappa_3 &\equiv (2 \log \sigma_0 + 0.4 \langle \mu \rangle_{\text{eff}} - \log R_{\text{eff}}) / \sqrt{3} \end{aligned} \quad (5)$$

where the quantities κ_i were constructed with the hope that κ_1 would be proportional to mass, κ_3 would be proportional to mass-to-light ratio, and κ_2 (which is required to be orthogonal to κ_1 and κ_3) would be proportional to the product of mass-to-light ratio and the third power of mean surface brightness. This “ κ –space” is displayed in Figure 4 for the K –band survey. Given the above interpretation of κ_1 and κ_3 , the fitted line between these two variables

$$\kappa_3 = 0.147 \kappa_1 + 5.721 \langle \mu_K \rangle_{\text{eff}} \quad N = 251 \quad \text{rms} = 0.068 \text{ dex} \pm 0.011 \quad \pm 0.038 \quad (6)$$

then implies that the “observed mass-to-light ratio”⁹ in the K -band varies as $(M/L_K) \propto M^{0.147 \pm 0.011} \propto L_K^{0.172 \pm 0.013}$. This conclusion is dependent on elliptical galaxies forming a dynamically homologous family in which the central velocity dispersion scales to the effective velocity dispersion (the velocity dispersion within the effective radius) independently of the mass or luminosity of the galaxy. The uncertainties in Equation 6 were derived using bootstrap resampling of the data points. The cumulative observational uncertainties in this equation are 0.033 dex in κ_3 , which is substantially smaller than the rms of the fit, implying a substantial intrinsic scatter of the “observed mass-to-light ratio” for any given “mass.”

While it is desirable to choose an orthogonal coordinate system which might directly relate the observables to underlying physical properties of elliptical galaxies, this conceptualization of the FP has a number of problems. First, the quantity R_{eff} is not equivalent to R_m , the half-mass radius, but instead varies with the observed wavelength. This generally follows from the presence of color gradients in elliptical galaxies (e.g., Franx, Illingworth, & Heckman 1989; Peletier *et al.* 1990a,b), but will be shown explicitly for the case of comparing V -band and K -band effective radii in the next paper in this series (Pahre, de Carvalho, & Djorgovski 1998). It follows that the value of κ_1 , which was intended to create a quantity which is proportional to mass, *systematically varies* as a function of wavelength while mass, of course, does not. Using the terminology of Djorgovski *et al.* (1988), the mapping from R_{eff} to gravitational radius R_g is accomplished in the equation $R_{\text{eff}} = k_R R_g$; the argument here is that the structure function k_R is not a constant, as is implicitly assumed in the construction of κ -space by Bender *et al.* (1992), but is instead a function of wavelength.

Second, while the evidence is not yet strong, the lowest luminosity ellipticals show no detectable color gradients (Peletier *et al.* 1990a), suggesting that there could be a dependence of the size of the color gradient on luminosity (and hence mass). The size of the color gradients also depends on the wavelength sampled (Franx *et al.* 1989; Peletier *et al.* 1990a,b). The mappings from κ_1 to mass and κ_3 to mass-to-light ratio are therefore a function of both wavelength and size of the color gradient (which is, in turn, a function of mass). Again using the terminology of Djorgovski *et al.* (1988), this means that the composite structure functions k_{SR} and k_{SL} (see their Equations 5–8) are also not constant, as is implied by the construction of κ -space, but are instead functions of wavelength and mass.

Third, the use of the central velocity dispersion σ_0 in deriving mass at the effective radius assumes dynamical homology among elliptical galaxies when mapping σ_0 (the central velocity dispersion) to σ_{eff} (the velocity dispersion within the effective radius). Whether or not the internal stellar velocity distributions of elliptical galaxies form a homologous family is a point of considerable debate. Empirical arguments (Jørgensen, Franx, & Kjærgaard 1995b, Busarello *et al.*

⁹For the reasons discussed later in this section, we prefer to distinguish between this observed relationship (between κ_1 and κ_3) and the *intrinsic* M and (M/L) ; the intrinsic properties may or may not be fully described by the axes κ_1 and κ_3 .

1997) and numerical simulations of dissipation-less merging (Capelato *et al.* 1995) seem to suggest that the way σ_0 scales to σ_{eff} is a function of galaxy mass or luminosity. The mapping from κ_1 to mass and κ_3 to mass-to-light ratio are therefore a function of mass or luminosity, and possibly a function of other physical processes which are currently poorly understood. Once again using the terminology of Djorgovski *et al.* (1988), the mapping from the intrinsic velocity distribution $\langle v^2 \rangle$ to the observed σ in the equation $\sigma^2 = k_V \langle v^2 \rangle$ is accompanied by a dependence of k_V on galaxy mass (or luminosity) and systematic deviations from a dynamical homology.

In summary, because the mapping from the observables to κ -space is a *function* of wavelength, luminosity, and deviations from dynamical homology, and furthermore because the mapping from κ -space to mass and mass-to-light ratio is also a *function* of wavelength, luminosity, and deviations from dynamical homology, we eschew the use of κ -space since it is an obfuscation, rather than an illumination, of the fundamental physical quantities of elliptical galaxies which we wish to understand. At its best, the κ -space formalism is merely an *intermediate* orthogonal transformation between the observables $[R_{\text{eff}}, \langle \mu \rangle_{\text{eff}}, \sigma_0]$ and the desired physical properties $[M, L, M/L(\lambda)]$.

3.4. The Mg_2 - σ_0 Relation

The Mg_2 - σ_0 relation is a correlation between two distance independent quantities and hence useful both as a diagnostic and as a constraint on formation processes for elliptical galaxies as a family. Guzmán (1995), for example, found that the residuals of the Mg_2 - σ_0 relation and the D - σ_0 relation showed systematic differences between the Hydra-Centaurus region and the Coma cluster, thereby suggesting that there are differences between the global properties of galaxies in those two environments.

Only a fraction of galaxies for which σ_0 is available also have Mg_2 values available. Of the entire sample of 301 early-type galaxies in these 16 clusters and groups, only 188 galaxies (62%) fit the criteria of $\log \sigma_0 \geq 1.8$ and have Mg_2 measurements. There are six galaxies at low σ_0 that show anomalously low Mg_2 and are therefore excluded: M32, NGC 3489 in the Leo Group, and NGC 4239, NGC 4468, NGC 4476, and NGC 4733 in the Virgo cluster (NGC 4489 was previously excluded for $\log \sigma_0 < 1.8$). Many of these are dwarf galaxies which are known to follow different FP correlations. The criterion used for this exclusion was that all galaxies satisfy $\text{Mg}_2 < \frac{5}{7}(2.2 - \log \sigma_0)$. The best fitting Mg_2 - σ_0 relation is

$$\begin{aligned} \text{Mg}_2(\text{ mag}) = & 0.173 \log \sigma_0 - 0.106 & N = 182 & \text{rms} = 0.019 \text{ mag} \\ & \pm 0.010 & & \pm 0.024 \end{aligned} \tag{7}$$

This relation is plotted in Figure 5. The slope of this relation is slightly shallower than the value of 0.196 ± 0.009 found by Jørgensen (1998), and the scatter is slightly smaller than the 0.025 mag of Jørgensen. Inclusion of the six galaxies anomalously low in Mg_2 and the one galaxy with $\log \sigma < 1.8$ produces a Mg_2 - σ_0 relation $\text{Mg}_2 = 0.188 \pm 0.012 \log \sigma_0 - 0.140 \pm 0.026$ with a scatter of

0.021 mag; this is closer to, and statistically indistinguishable from, Jørgensen’s results. The form in Equation 7 will be used, however, as it best represents the properties of the normal elliptical galaxies.

3.5. The Mg_2 Near-Infrared Fundamental Plane

An alternative form of the FP was proposed by de Carvalho & Djorgovski (1989): substitute a stellar populations indicator, such as the Mg_2 index, for the dynamical or mass indicator σ_0 in the FP relation. The motivation for this is that since Mg_2 and σ_0 are strongly correlated with each other (as shown above in §3.4) then metallicity could actually be the fundamental physical property that causes the slope of the FP to deviate from the virial expectation. de Carvalho & Djorgovski also showed that a metallicity sensitive color could be substituted for σ_0 , although that approach will not be pursued here due to the heterogeneity of the derived optical–infrared colors in Paper II (see Pahre 1998).¹⁰ The resulting FP in the near-infrared K -band using the Mg_2 index in place of $\log \sigma_0$ is

$$\log r_{\text{eff}}(\text{arcsec}) = \begin{array}{l} 8.3 \text{ } Mg_2 + \quad 0.324 \langle \mu_K \rangle_{\text{eff}} + c_i \quad N = 181 \quad \text{rms} = 0.172 \text{ dex} \\ \pm 0.9 \quad \quad \quad \pm 0.015 \end{array} \quad (8)$$

The slope of this relation is 8.3 ± 0.9 , as predicted by the slope of the Mg_2 – σ_0 relation combined with the standard form of the near-infrared FP, i.e., $(1.53 \pm 0.08)/(0.173 \pm 0.010) = 8.8 \pm 0.7$. The observational uncertainties increase when Mg_2 is used instead of $\log \sigma_0$ since the latter quantity has ~ 3 times greater uncertainty, while the slope has changed by more than a factor of five from Equation 2 to Equation 8. The scatter in the near-infrared Mg_2 FP, however, has increased by much more than this difference, suggesting that Mg_2 is not nearly as good an indicator as the velocity dispersion in describing the fundamental and regular physical properties in elliptical galaxies that give rise to the FP. The Mg_2 index could be identifying real differences in the stellar populations among galaxies and hence shows larger scatter when it is substituted into the FP.

If part of the scatter in the r_{eff} – $\langle \mu_K \rangle_{\text{eff}}$ – σ_0 FP can be attributed to differences in stellar populations among elliptical galaxies, then the introduction of a stellar populations “correction” factor based on the Mg_2 index should be able to reduce the scatter of the FP even though a small amount of additional observational uncertainty is added in the process. The idea for this

¹⁰Basically, the fundamental requirement for such an investigation of the “color FP” is to understand the difference between an “aperture” color–magnitude relation, the standard form which relies on a color measured in a fixed physical aperture size for all galaxies, and a “global” color–magnitude relation, which is evaluated at some fiducial scaling radius. Part of the slope of the “aperture” color–magnitude relation is certainly due to the presence of color gradients which act in the sense that ellipticals are redder in their centers: the smallest galaxies have their colors evaluated at large r/r_{eff} where their color is bluer, while the largest galaxies have their colors evaluated at small r/r_{eff} where their color is redder. Future work should explicitly distinguish between the two effects of color gradients and global color differences in order to place a constraint on the global properties of ellipticals.

comes from the attempt by Guzmán & Lucey (1993) to construct an “age-independent” distance indicator. Here the method will be applied to the near-infrared data.

Using Bruzual (1983) evolutionary spectral synthesis models, Guzmán & Lucey showed that the effects of a burst of star formation involving 10% of a galaxy’s mass would appear as a change of $\Delta m/\Delta \text{Mg}_2$ roughly constant for times $\gtrsim 1$ Gyr or so after the burst. Hence, an offset in magnitude Δm could be applied to each galaxy independently based on its departure ΔMg_2 from the $\text{Mg}_2\text{-}\sigma_0$ relation. Guzmán & Lucey also showed that while the effect in the optical V -band was $\Delta m_V/\Delta \text{Mg}_2 \sim 10$, the effect in the near-infrared was much smaller at

$$\frac{\Delta m_K}{\Delta \text{Mg}_2} \sim 2. \quad (9)$$

This effect can basically be understood as a filling-in of the Mg_2 feature by the addition of a continuum flux from hot, young stars. The changes in the Mg_2 index are expected to be small, as Mg_2 is far more sensitive to metallicity than it is to age or IMF (Mould 1978).

The Guzmán & Lucey procedure is repeated here for the Worthey (1994) stellar populations models in order to determine if the size of the predicted age effects are similar despite significant differences between the Bruzual (1983) and Worthey (1994) models. The model adopted is similar to Guzmán & Lucey in that it involves $10^6 M_\odot$ total mass, 90% of which is 15 Gyr old in the present day, 10% of which is 5 Gyr old, and all of which has solar metallicity. A similar model is investigated that involves 90% of the galaxy being 11 Gyr old in the present day and 10% being 5 Gyr old. The results from the Worthey models are plotted in Figure 7 for the $UBVR$ bandpasses.

The Worthey models show modest agreement with the Guzmán & Lucey calculations based on Bruzual (1983) models for the optical bandpasses, although the value of $\Delta \text{mag}/\Delta \text{Mg}_2$ is systematically 30–50% higher. In the K -band, however, Worthey’s models are 3–4 times higher in this quantity. The most likely explanation for this is the difficulty that many models have in producing enough Mg relative to Fe for very metal-rich populations (see Worthey, González, & Faber 1992, for example), although more fundamental problems in the treatment of cool stellar atmospheres in the infrared for the Worthey models (see Charlot, Worthey, & Bressan 1996) could also be relevant. As a result of this discrepancy, the effects of a late burst of star formation involving a small fraction of the galaxy mass on the FP cannot be assumed *a priori*.

A better approach is to measure directly the possible contribution of younger stellar populations using the FP itself, and then using the observations to constrain the models. Combining Equations 1 and 7, defining $r_K = \frac{\Delta m_K}{\Delta \text{Mg}_2}$, and assuming that the mean surface brightness term in the FP is the only one affected by r_K yields:

$$\log r_{\text{eff}}(\text{arcsec}) = a' \log \sigma_0 + b' (\langle \mu_K \rangle_{\text{eff}} - r_K [\text{Mg}_2 - 0.173 \log \sigma_0 + 0.106]) + c_i \quad (10)$$

where the primed coefficients are the “age-independent” form of the FP. The Guzmán & Lucey analysis predicts $r_K \sim 2$, while the Worthey models predict $r_K \sim 7$.

Unfortunately, a minimization of Equation 10 does not reveal an optimal value of r_K since values of $|r_K| > 0$ increase the scatter of the equation due to the added measurement uncertainties. Put another way, there was no significant improvement in the scatter (by $> 2\%$) of the FP for any r_K in the range $-10 < r_K < +10$. Since the intrinsic thickness of the near-infrared FP is clearly resolved without including a Mg_2 term (i.e., Equation 2 and Figure 2), then some of that thickness could be due to variations in age among the stellar populations of elliptical galaxies. This effect can be viewed from a similar perspective by attempting to correlate the residuals of the near-infrared FP with the residuals of the $Mg_2-\sigma_0$ relation. This $\Delta-\Delta$ diagram is shown in Figure 8. This figure shows no correlation among the residuals in the direction of the age vectors, implying that the resolved intrinsic scatter of both the near-infrared FP and the $Mg_2-\sigma_0$ relations cannot be caused by age effects alone.

Instead, insight can be gained by looking for changes in the relative distance modulus between a given cluster and the Coma cluster. When $r_K = 2$, all 16 clusters and groups show changes in their distance moduli relative to Coma of ≤ 0.05 mag, which is smaller than the typical uncertainty of 0.1 mag in the distance to a cluster of $N = 20$ galaxies for a scatter of $\log r_{\text{eff}} = 0.085$ dex. The difference in relative distance modulus between the $r_K = 0$ and $r_K = 7$ cases, however, reach as high as 0.12–0.18 mag in the case of several clusters (Virgo, Cen30, and Pegasus), which is marginally significant. Since the Worthey (1994) models probably overestimate r_K due to their difficulty in producing Mg for metal-rich populations, the conclusion is that 0.18 mag is a firm upper limit to the effects of age differences on the distance moduli derived using the near-infrared FP. This result for the K -band is similar to that found in the r -band by Jørgensen *et al.* (1996), who found a minimally-significant contribution of $r_r = 1.3 \pm 0.8$. They probably found no good correlation for the reason given above—that the increase of measurement uncertainties as r increases prevents effective minimization during the fitting—hence this may not be a significant constraint on a superimposed intermediate age contribution. Repeating the analysis using $r_V = 10$ for the Abell 2199 and Abell 2634 clusters for the galaxies in the V and K matched catalog produces a similarly small change in their distance moduli relative to Coma. In summary, there is little evidence that adding a Mg_2 term (based on the $Mg_2-\sigma_0$ relation) to the near-infrared FP to account for age differences in the ellipticals in different clusters causes a significant improvement over the zero-point for the relation and hence distances derived from it.

A similar approach could be pursued by looking at the correlation between the residuals of the $Mg_2-\sigma_0$ relation and the residuals of the $\kappa_3-\kappa_1$ relation. If differences of Mg_2 at a fixed σ_0 indicate differences of stellar populations, and if differences of κ_3 at a fixed κ_1 indicate differences in (M/L) due to stellar populations effects, then the residuals of these two relations (Equations 10 and 6) should correlate in a manner that is consistent with stellar populations effects. These residuals are plotted against each other in Figure 9.

This figure is an excellent diagnostic for distinguishing between age and metallicity effects, since Mg_2 decreases for younger stellar populations while it increases for higher metallicities, but (M/L_K) decreases for both. [If the vertical axis were $\Delta(M/L)$ measured at any optical

wavelength, then age and metallicity would instead act nearly parallel.] The lack of any preferred correlation along either the age or metallicity vectors in Figure 9, while at the same time having a substantial intrinsic scatter for both relations, strongly indicates that both age and metallicity variations exist at any given point on both the Mg_2 and $\kappa_3\text{-}\kappa_1$ relations.

The $\text{H}\beta$ index is expected to be a good indicator of the presence of a young stellar component, and either the Mg_2 or $\log\langle\text{Fe}\rangle$ indices should be good indicators of the mean metallicity of the stellar content. The large intrinsic scatter between the $\text{H}\beta$ and Mg_2 indices, the lack of a correlation altogether between $\text{H}\beta$ and $\log\langle\text{Fe}\rangle$, the strong correlation between Mg_2 and σ_0 , and the weak correlation between $\log\langle\text{Fe}\rangle$ and σ_0 (Jørgensen 1998) all indicate that there exist significant variations in both age and metallicity for any given value of σ_0 . This is fully consistent with the argument above based on the residuals of the $\text{Mg}_2\text{-}\sigma_0$ and $\kappa_3\text{-}\kappa_1$ relations.

3.6. The Faber–Jackson Relation

The correlation between luminosity and central velocity dispersion for elliptical galaxies was first noticed by Faber & Jackson (1976). If we fit the relation $L \propto \sigma_0^a$, this is equivalent to fitting $K_{\text{tot}} = -2.5a \log \sigma_0 + b$. The best fitting Faber–Jackson relation for the K -band data is

$$M_K = K_{\text{tot}} - 34.91 + 5 \log h_{75} = -10.35 \log \sigma_0 \quad N = 252 \quad \text{rms} = 0.93 \text{ mag} \quad (11)$$

± 0.55

assuming $H_0 = 75 \text{ km s}^{-1}$ and that the Coma cluster ($cz = 7200 \text{ km s}^{-1}$) is at rest with respect to the Hubble flow. The relation is plotted in Figure 10. The scatter of this relation is significantly smaller in the Coma cluster alone (rms= 0.72 mag).

3.7. The Modified Faber–Jackson Form of the FP

Since there is substantial scatter in the Faber–Jackson relation due to variations in surface brightness among galaxies at a given luminosity and central velocity dispersion, an alternate form of the FP is to substitute K_{tot} for r_{eff} . This will be referred to as the “modified Faber–Jackson” relation, as it adds the additional $\langle\mu\rangle_{\text{eff}}$ term to the Faber–Jackson relation. The form of this equation is

$$K_{\text{tot}} = a' \log \sigma_0 (\text{km s}^{-1}) + b' \langle\mu\rangle_{\text{eff}} (\text{mag arcsec}^{-2}) + c'_i \quad (12)$$

where the primed coefficients are used here for the modified Faber–Jackson relation. Since in the case of a pure de Vaucouleurs profile $K_{\text{tot}}(\text{mag}) = -5 \log r_{\text{eff}} + \langle\mu_K\rangle_{\text{eff}} - 1.995$, the value $\log r_{\text{eff}} = a \log \sigma_0 + b \langle\mu_K\rangle_{\text{eff}} + \text{constant}$ can be substituted for r_{eff} resulting in $a = -5a'$ and $b = 0.2(1 - b')$, thereby relating Equations 1 and 12 to each other. The best-fitting relation of the

modified Faber–Jackson form of the FP is:

$$M_K + 5 \log h_{75} = -8.16 \log \sigma_0 - 0.585 \langle \mu_K \rangle_{\text{eff}} + c_i \quad N = 251 \quad \text{rms} = 0.51 \text{ mag} \quad (13)$$

$$\pm 0.47 \quad \pm 0.062$$

which has a scatter only 10% larger than the standard form of the near–infrared FP given in Equation 2. This equation represents the scaling relation $L_K \propto \sigma_0^{3.26 \pm 0.19} \langle \Sigma_K \rangle_{\text{eff}}^{-0.59 \pm 0.06}$, which is fully equivalent within the uncertainties to the standard form of the near–infrared FP. Since the uncertainty on $K_{\text{tot}} + 0.60 \langle \mu_K \rangle_{\text{eff}}$ is 0.068 mag, the total observational uncertainties in Equation 2 and 13 are similar. Hence Equation 13 also shows substantial intrinsic scatter in the properties of elliptical galaxies at any point along the FP.

3.8. The Kormendy Relation

Effective radius and mean surface brightness, which are two of the three terms in the FP, are correlated with each other (Kormendy 1977). The best fitting Kormendy relation for the K –band data is

$$\log R_{\text{eff}} h_{75}^{-1} = 0.244 \langle \mu_K \rangle_{\text{eff}} - 3.637 \quad N = 269 \quad \text{rms} = 0.227 \text{ dex} \quad (14)$$

$$\pm 0.029$$

assuming $H_0 = 75 \text{ km s}^{-1}$ and that the Coma cluster ($cz = 7200 \text{ km s}^{-1}$) is at rest with respect to the Hubble flow. The relation is plotted in Figure 12. The scatter of this relation is significantly smaller in the Coma cluster alone (rms= 0.198 dex). Measurement errors in r_{eff} and $\langle \mu \rangle_{\text{eff}}$ are correlated and act in a direction nearly parallel to the Kormendy relation, but are not nearly large enough to account for the spread in galaxy properties along the relation. Changes in luminosity are skewed with respect to this relation and shown in Figure 12. For this reason it is necessary that a magnitude–limited sample be defined in a consistent way for all clusters studied before conclusions based on changes in the zero–point (due to distances for nearby clusters or evolutionary brightening for higher redshifts) can be made.

3.9. The Radius–Luminosity Relation

The correlation between the effective radius and total magnitude for elliptical galaxies has long been used for distance scale work and especially cosmological tests (see Sandage & Perelmuter 1990 and references therein). The best fitting radius–luminosity relation for the K –band data is

$$M_K + 5 \log h_{75} = -4.40 R_{\text{eff}} - 22.31 \quad N = 269 \quad \text{rms} = 0.88 \text{ mag} \quad (15)$$

$$\pm 0.26$$

assuming $H_0 = 75 \text{ km s}^{-1}$ and that the Coma cluster ($cz = 7200 \text{ km s}^{-1}$) is at rest with respect to the Hubble flow. The relation is plotted as Figure 13. There is intrinsic scatter to this relation that is a result of the variation in surface brightness at a given radius and luminosity; lines of constant surface brightness are plotted in the figure to demonstrate this effect.

4. Exploring Simple Models for the Origins of the Elliptical Galaxy Scaling Relations in the Near-Infrared

The near-infrared FP has been shown in §3.1 to be represented by the scaling relation $r_{\text{eff}} \propto \sigma_0^{1.53 \pm 0.08} \langle \Sigma_K \rangle_{\text{eff}}^{-0.79 \pm 0.03}$. This relation shows a significant deviation from the optical forms of the FP: $r_{\text{eff}} \propto \sigma_0^{1.24 \pm 0.07} \langle \Sigma \rangle_{\text{eff}}^{-0.82 \pm 0.02}$ (Jørgensen, Franx, & Kjaergaard 1996) and $r_{\text{eff}} \propto \sigma_0^{1.38 \pm 0.04} \langle \Sigma \rangle_{\text{eff}}^{-0.82 \pm 0.03}$ (Hudson *et al.* 1997) in the R -band; or $r_{\text{eff}} \propto \sigma_0^{1.13} \langle \Sigma \rangle_{\text{eff}}^{-0.79}$ in the V -band (Guzmán, Lucey, & Bower 1993). There are two simple conclusions to draw from these data: (1) the slope of the near-infrared FP deviates from the virial expectation of $r_{\text{eff}} \propto \sigma_0^2 \langle \Sigma \rangle_{\text{eff}}^{-1}$, and (2) the slope of the FP increases with wavelength. A third insight derives from the fact that the scatter of the FP is very similar at all wavelengths. These three points are sufficient to discuss several simple models for the physical origins of the FP.

The age-metallicity model of Worthey, Trager, & Faber (1995)—based on the form of the FP in the optical, various line indices, and simple stellar populations model comparisons—incorrectly predicts that the near-infrared FP should follow the virial form. Another model, that the FP slope is caused by deviations of the velocity distributions of elliptical galaxies from a homologous scaling family (Capelato *et al.* 1995), cannot account for the variations of the slope of the FP with wavelength. If this breaking of homology has its origin in dissipation-less merging, then this effect also cannot explain the correlation between Mg_2 and σ_0 . A final model, which suggests that deviations of the light distributions of elliptical galaxies from the de Vaucouleurs $r^{1/4}$ form is the cause of the FP slope, is unable to account for the slope of the FP in the optical (Graham & Colless 1997), and for the same reasons it cannot explain the near-infrared FP slope.

The deviation of the slope of the near-infrared FP from the virial expectation, assuming homology and constant M/L among ellipticals, is a very significant result. This requires a breakdown of one or both assumptions: either M/L is systematically varying along the FP, or elliptical galaxies are systematically deviating from a homologous scaling family. If age is the stellar populations parameter which causes variations in the slope of the FP with wavelength, then age alone might possibly produce the slope of the K -band FP. This conclusion, however, is severely limited by the possibility of homology breaking along the elliptical galaxy sequence.

Allowing for structural deviations from homology, in the form of a Sersic $r^{1/n}$ profile, does not appear to cause significant changes to the slope of the FP for high S/N, V -band data in the Virgo cluster (Graham & Colless 1997). Instead, allowing for dynamical deviations from homology, via galaxy to galaxy variations in the mapping from σ_0 to σ_{eff} , appears to cause significant changes in the slope of the FP (Busarello *et al.* 1997; cf. Graham & Colless 1997). Busarello *et al.* found a relationship between the velocity dispersions to be $\log \sigma_0 = (1.28 \pm 0.11) \log \sigma_{\text{eff}} - 0.58$. Substituting for $\log \sigma_0$ into the K -band FP solution in Equation 2 produces

$$\log r_{\text{eff}} = \begin{array}{l} 1.96 \log \sigma_{\text{eff}} + 0.314 \langle \mu_K \rangle_{\text{eff}} + \text{constant} \\ \pm 0.20 \qquad \qquad \pm 0.011 \end{array} \quad (16)$$

which is statistically consistent with the virial expectation of $r_{\text{eff}} \propto \sigma^2$. This argument suggests

that the deviation of the near-infrared FP from the virial expectation can be fully explained by systematic deviations of the velocity structure of elliptical galaxies from a homologous family, removing the requirement of large age spreads among elliptical galaxies.

Since either dynamical non-homology or large age spreads could produce the slope of the near-infrared FP, it is impossible to distinguish between these two simple models without further analysis. In addition, any model which incorporates either age or dynamical deviations from a homology along with metallicity variations cannot be excluded in this simple analysis, either. This strongly suggests that a much more detailed analysis, along with a more complicated model with several different variables, is necessary to explain the global properties of elliptical galaxies.

One last *ad hoc* model can be constructed in which there is a *conspiracy* between metallicity and age effects that act in a manner to keep the FP thin. In this model, there can be a large spread in age and metallicity at any given point of the FP—under the constraint that the two effects of age and metallicity work opposite to each other and thereby cancel out to maintain a small scatter. While this model would work at optical wavelengths, the independence of near-infrared light to metallicity would cause the thinness of the optical FP to break down into a thick, near-infrared FP. Since the near-infrared FP has similar observed and intrinsic thicknesses when compared to the optical FP, especially when considering the additional observational uncertainties on r_{eff} caused by σ_0 for the steeper slope of the near-infrared FP, this model can be excluded.

5. Discussion

The near-infrared FP that has been constructed in this paper has several important properties: (1) it deviates from the virial expectation (assuming constant M/L and homology); (2) it is steeper than the optical FP relations; (3) it has a similarly small scatter when compared to the optical FP relations; and (4) it has a small, but significantly resolved, intrinsic scatter. These observational constraints are sufficient to exclude a number of simple models for the origin of the FP, but they do not provide unique discrimination between composite models which include either age, systematic deviations from dynamical homology, or both. Small additional contributions due to metallicity variations are also possible.

Better insight is gained by including the Mg_2 index into the analysis. The Mg_2 form of the FP has much larger scatter than the standard form, which argues that Mg_2 does not uniquely specify the depth of the potential well for each galaxy. This is entirely consistent with the resolved intrinsic scatter of the Mg_2 - σ_0 relation. If some physical process like galactic winds (Yoshii & Arimoto 1987) caused the metallicity and potential well for all elliptical galaxies to behave like a one-parameter family, then some other physical property, such as dissipation-less mergers or a large scatter in formation times, would be required to produce the small intrinsic scatter of the Mg_2 - σ_0 relation and the large intrinsic scatter of the Mg_2 form of the FP.

The near-infrared FP has the unique property that the K -band light is virtually independent

of metallicity. For this reason, residuals of the K -band FP (or the K -band relationship between κ_1 and κ_3) and the $Mg_2-\sigma_0$ relations could provide a strong discrimination between age and metallicity effects. The lack of any clear correlation between these residuals implies that neither age nor metallicity is a unique contributor to the intrinsic scatter of the FP or the $Mg_2-\sigma_0$ relations.

The Fundamental Plane is not just a simple correlation of the observed properties of elliptical galaxies, but rather a unique tool for studying the intrinsic physical properties spanned by these galaxies. The remarkable homogeneity of properties of elliptical galaxies that is implied by the regularity and thinness of the optical FP is clearly reproduced by their similarly regular properties in the near-infrared bandpass.

J. Blakeslee and J. Tonry are thanked for providing their SBF distance moduli in electronic form. This research has made use of the NASA/IPAC Extragalactic Database (NED) which is operated by the Jet Propulsion Laboratory, California Institute of Technology, under contract with the National Aeronautics and Space Administration. During the course of this project, M. A. P. received financial support from Jesse Greenstein and Kingsley Fellowships, and Hubble Fellowship grant HF-01099.01-97A from STScI (which is operated by AURA under NASA contract NAS5-26555); S. G. D. was supported in part by grants from the NSF (AST-9157412) and the Bressler Foundation.

Table 1. Fits for Each Cluster or Group for the Near-Infrared FP

Cluster or Group	Simultaneous Fit			Individual Fits					Constrained $b = 0.314$ Fits		
	c_i	N	rms (dex)	a	Δa	b	Δb	rms (dex)	a	Δa	rms (dex)
(1)	(2)	(3)	(4)	(5)	(6)	(7)	(8)	(9)	(10)	(11)	(12)
Coma	-7.950	60	0.086	1.33	0.19	0.302	0.03	0.082	1.57	0.15	0.088
A194	-7.734	16	0.107	1.57	0.21	0.254	0.05	0.106	1.60	0.16	0.110
A2199	-8.128	23	0.093	1.53	0.22	0.342	0.03	0.088	1.40	0.16	0.086
A2634	-8.028	15	0.076	1.19	0.74	0.292	0.06	0.061	1.24	0.30	0.063
Cen45	-7.543	6	0.071
Cen30	-7.526	14	0.124	1.72	0.41	0.299	0.08	0.123	2.05	0.39	0.139
Fornax	-7.274	15	0.137	2.56	0.65	0.339	0.06	0.156	2.11	0.30	0.128
Hydra	-7.669	17	0.086	1.76	0.34	0.344	0.03	0.080	1.77	0.15	0.086
Klemola 44	-8.041	11	0.067	1.50	0.58	0.309	0.05	0.068	1.74	0.28	0.069
Pegasus	-7.580	4	0.048
Perseus	-7.802	19	0.100	1.98	0.59	0.310	0.05	0.125	1.66	0.33	0.104
Pisces	-7.723	11	0.087	1.04	0.27	0.350	0.05	0.055	1.17	0.19	0.055
Virgo	-7.175	27	0.115	1.77	0.25	0.374	0.03	0.120	1.62	0.12	0.118
Eridanus	-7.312	5	0.061
Leo	-6.932	3	0.253
N5846grp	-7.436	5	0.101

Note. — (1) The FP fits in this table are to the form of Equation 1. (2) The simultaneous fit for columns 2–4 corresponds to the solution in Equation 2, allowing only the intercepts c_i to vary between clusters. (3) The individual cluster FP fits in columns 5–9 are for only those 11 clusters with numbers of galaxies $N \geq 10$. (4) The constrained, individual cluster fits of columns 10–12 were obtained by fixing $b = 0.314$. (5) The rms in all cases is evaluated along the $\log r_{\text{eff}}$ axis.

REFERENCES

- Baum, W. A. 1959, *PASP*, 71, 106
- Bender, R., Burstein, D., & Faber, S. M. 1992, *ApJ*, 399, 462
- Bower, R. G., Lucey, J. R., & Ellis, R. S. 1992, *MNRAS*, 254, 601
- Bruzual, A. G. 1983, *ApJ*, 273, 105
- Busarello, G., Capaccioli, M., Capozziello, S., Longo, G., & Puddu, E. 1997, *A&A*, 320, 415
- Capelato, H. V., de Carvalho, R. R., & Carlberg, R. G. 1995, *ApJ*, 451, 525
- Capelato, H. V., de Carvalho, R. R., & Carlberg, R. G. 1997, in *Galaxy Scaling Relations: Origins, Evolution, and Applications*, Proceedings of the Third ESO–VLT Workshop, eds. L. N. da Costa & A. Renzini (Springer–Verlag: Berlin), 331
- de Carvalho, R. R., & Djorgovski, S. 1989, *ApJ*, 341, L37
- Charlot, S., Worthey, G., & Bressan, A. 1996, *ApJ*, 457, 625
- Ciotti, L., Lanzoni, B., & Renzini, A. 1996, *MNRAS*, 282, 1
- Djorgovski, S. G., de Carvalho, R., & Han, M.-S. 1988, in *The Extragalactic Distance Scale*, ASP Conf. Ser. Vol. 24, eds. S. van den Bergh & C. J. Pritchet (San Francisco, ASP), 329
- Djorgovski, S., & Davis, M. 1987, *ApJ*, 313, 59
- Djorgovski, S., & Santiago, B. X. 1993, in *Proceedings of the ESO/EIPC Workshop on Structure, Dynamics, and Chemical Evolution of Early–Type Galaxies*, ed. J. Danziger, *et al.*, ESO publication No. 45, 59
- Dressler, A. 1984, *ApJ*, 281, 512
- Dressler, A., Lynden–Bell, D., Burstein, D., Davies, R. L., Faber, S. M., Terlevich, R. J., & Wegner, G. 1987, *ApJ*, 313, 42
- Faber, S. M., & Jackson, R. E. 1976, *ApJ*, 204, 668
- Franx, M., Illingworth, G., & Heckman, T. 1989, *AJ*, 98, 538
- Graham, A., & Colless, M. 1997, *MNRAS*, 287, 221
- Guzmán, R., Lucey, J. R., & Bower, R. G. 1993, *MNRAS*, 265, 731
- Guzmán, R. 1995, in *Proceedings of the Heron Island Workshop on Peculiar Velocities in the Universe*, <http://qso.lanl.gov/~heron/>

- Hudson, M. J., Lucey, J. R., Smith, R. J., & Steel, J. 1997, MNRAS, in press
- Jefferys, W. H., Fitzpatrick, M. J., McArthur, B. E., and McCartney, J. E. 1987, “GaussFit: A System for Least Squares and Robust Estimation,” The University of Texas at Austin
- Jørgensen, I. 1998, MNRAS, in press
- Jørgensen, I., Franx, M., & Kjaergaard, P. 1995a, MNRAS, 273, 1097
- Jørgensen, I., Franx, M., & Kjaergaard, P. 1995b, MNRAS, 276, 1341
- Jørgensen, I., Franx, M., & Kjaergaard, P. 1996, MNRAS, 280, 167
- Kormendy, J. 1977, ApJ, 218, 333
- Lucey, J. R., & Carter, D. 1988, MNRAS, 235, 1177
- Lynden–Bell, D., Faber, S. M., Burstein, D., Davies, R. L., Dressler, A., Terlevich, R. J., & Wegner, G. 1988, ApJ, 326, 19
- Mould, J. R. 1978, ApJ, 220, 434
- Murphy, D. C., Persson, S. E., Pahre, M. A., Sivaramakrishnan, A., & Djorgovski, S. G. 1995, PASP, 107, 1234
- Pahre, M. A. 1998, ApJS, submitted
- Pahre, M. A., de Carvalho, R. R., & Djorgovski, S. G. 1998, AJ, submitted
- Pahre, M. A., & Djorgovski, S. G. 1997, in *The Nature of Elliptical Galaxies*, Proceedings of the Second Stromlo Symposium, eds. M. Arnaboldi, G. S. Da Costa, & P. Saha, ASP Conf. Ser. Vol. 116, (San Francisco: ASP), 154
- Pahre, M. A., Djorgovski, S. G., & de Carvalho, R. R. 1995, ApJ, 453, L17
- Pahre, M. A., Djorgovski, S. G., & de Carvalho, R. R. 1997, in *Galaxy Scaling Relations: Origins, Evolution, and Applications*, Proceedings of the Third ESO–VLT Workshop, eds. L. N. da Costa & A. Renzini (Springer–Verlag: Berlin), 197
- Peletier, R. F., Davies, R. L., Illingworth, G. D., Davis, L. E., & Cawson, M. 1990a, AJ, 100, 1091
- Peletier, R. F., Valentijn, E. A., & Jameson, R. F. 1990b, A&A, 233, 62
- Persson, S. E., Frogel, J. A., & Aaronson, M. 1979, ApJS, 39, 61
- Recillas-Cruz, E., Carrasco, L., Serrano, P. G., & Cruz-González, I. 1990, A&A, 229, 64
- Recillas-Cruz, E., Carrasco, L., Serrano, P. G., & Cruz-González, I. 1991, A&A, 249, 312

- Sandage, A. 1972, *ApJ*, 176, 21
- Sandage, A., & Visvanathan, N. 1978, *ApJ*, 223, 707
- Sandage, A., & Visvanathan, N. 1978, *ApJ*, 228, 81
- Sandage, A., & Perelmuter, J.-M. 1990, *ApJ*, 361, 1
- Smith, R. J., Lucey, J. R., Hudson, M. J., & Steel, J. 1997, *MNRAS*, in press
- Terlevich, R. J., Davies, R. L., Faber, S. M., & Burstein, D. 1981, *MNRAS*, 196, 381
- Tonry, J. L., & Davis, J. 1981, *ApJ*, 246, 680
- Tonry, J. L., Blakeslee, J. P., Ajhar, E. A., & Dressler, A. 1997, *ApJ*, 475, 399
- Visvanathan, N., & Sandage, A. 1977, *ApJ*, 216, 214
- Worthey, G. 1994, *ApJS*, 95, 107
- Worthey, G., González, J. J., & Faber, S. M. 1992, *ApJS*, 398, 69
- Worthey, G., Trager, S. C., & Faber, S. M. 1995, in *Fresh Views of Elliptical Galaxies*, ASP Conf. Ser. Vol. 86, eds. A. Buzzoni & A. Renzini (San Francisco: ASP) 203
- Yoshii, Y., & Arimoto, N. 1987, *A&A*, 188, 13

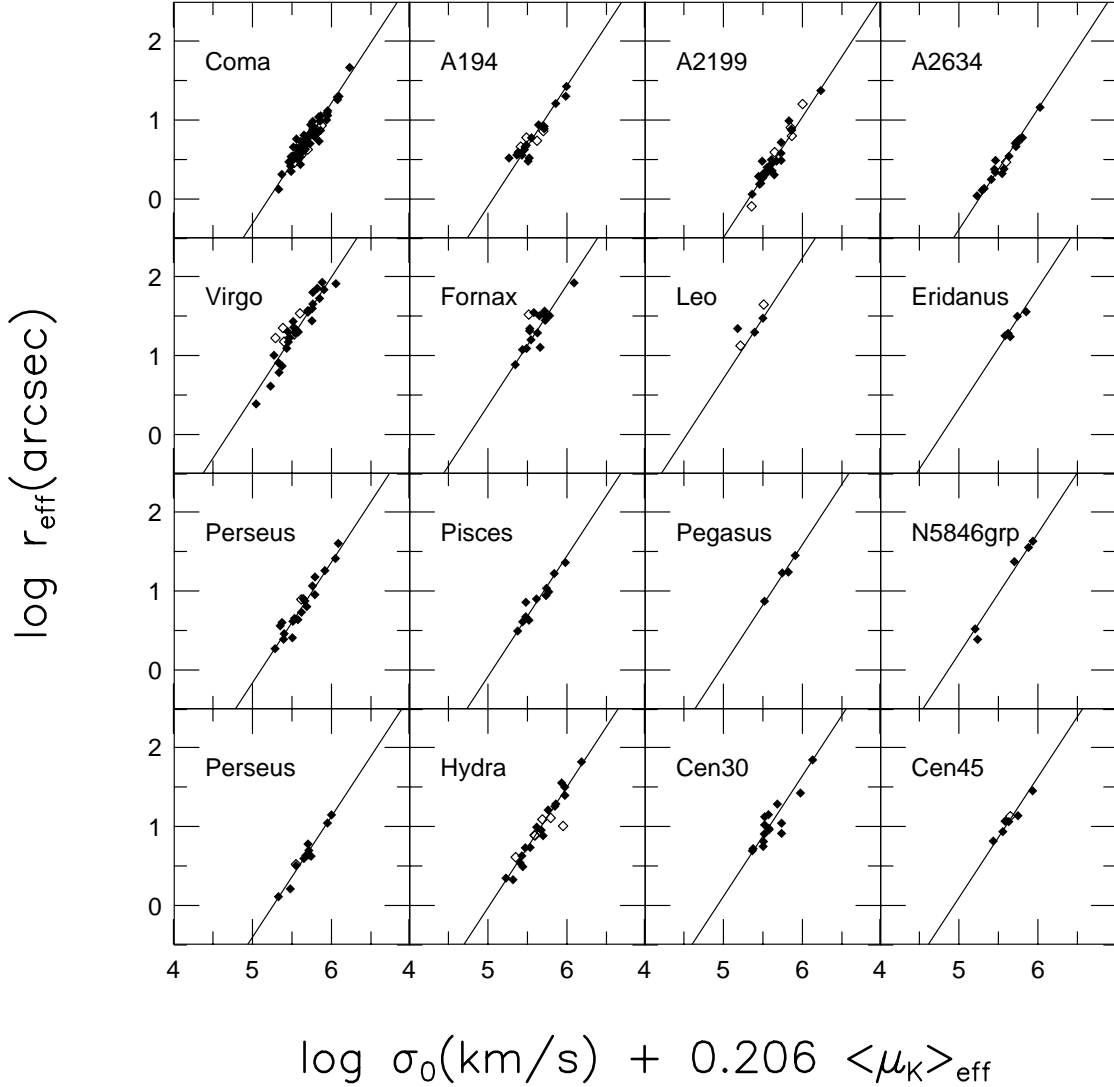


Fig. 1.— The Fundamental Plane in the near-infrared for the 16 clusters and groups in the simultaneous fit represented by the solution of Equation 2 and the intercepts in column 2 of Table 1. The FP is described by the scaling relation $r_{\text{eff}} \propto \sigma_0^{1.53} \langle \Sigma_K \rangle_{\text{eff}}^{-0.79}$ with a scatter of 0.096 dex in $\log r_{\text{eff}}$; the scatter is reduced by 10% of the galaxies with $\sigma_0 < 100 \text{ km s}^{-1}$ are excluded. The fitted galaxies are plotted as solid symbols, while those excluded from the fit ($\log \sigma_0 < 1.8$, late-type morphology, $r_{\text{eff}} < 1 \text{ arcsec}$, or background/foreground in the Virgo cluster) are plotted as open symbols. The FP fit is plotted in each panel as a solid line.

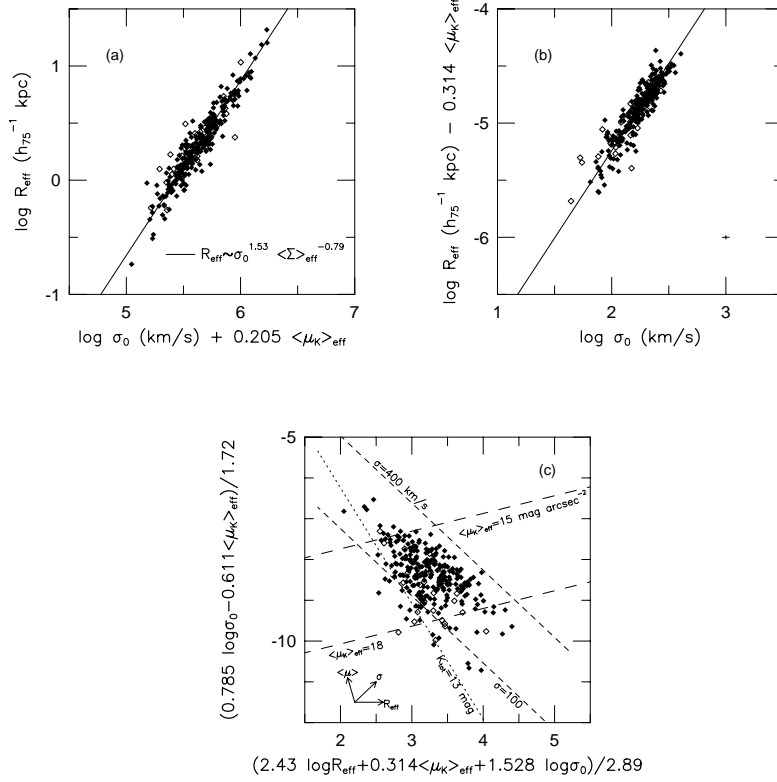


Fig. 2.— (a) The Fundamental Plane in the K -band for the combined 16 cluster and group sample, seen edge-on along its long side. The symbols are as in Figure 1. The ordinate is in units of kpc assuming $H_0 = 75 \text{ km s Mpc}^{-1}$. (b) The FP in the K -band for the combined 16 cluster and group sample, seen edge-on along its short side. In this view of the FP, the observationally-correlated measurement errors in R_{eff} and $\langle \mu_K \rangle_{\text{eff}}$ (ordinate) are separated from the independent measurement uncertainties in σ_0 (abscissa); the typical measurement uncertainties are shown in the lower right-hand corner of the panel. (c) The FP seen face-on. Galaxies do not uniformly populate this planar surface. While the K -band data in this paper are not drawn from a strictly magnitude-limited sample, they do behave as though a $K_{\text{tot}} \lesssim 13 \text{ mag}$ limit (dotted line) were imposed. Most of the galaxies are found to have $15 < \langle \mu_K \rangle_{\text{eff}} < 18 \text{ mag arcsec}^{-2}$ (long-dashed lines), although there are no clear selection effects causing this distribution of galaxy properties. Furthermore, there are no galaxies with properties in the upper-right portion of the figure, which could be caused by the lack of galaxies with velocity dispersions $\sigma_0 > 400 \text{ km s}^{-1}$ (short-dashed line). The vectors drawn in the lower left-hand corner show the direction in which each of the observed quantities varies along the plane.

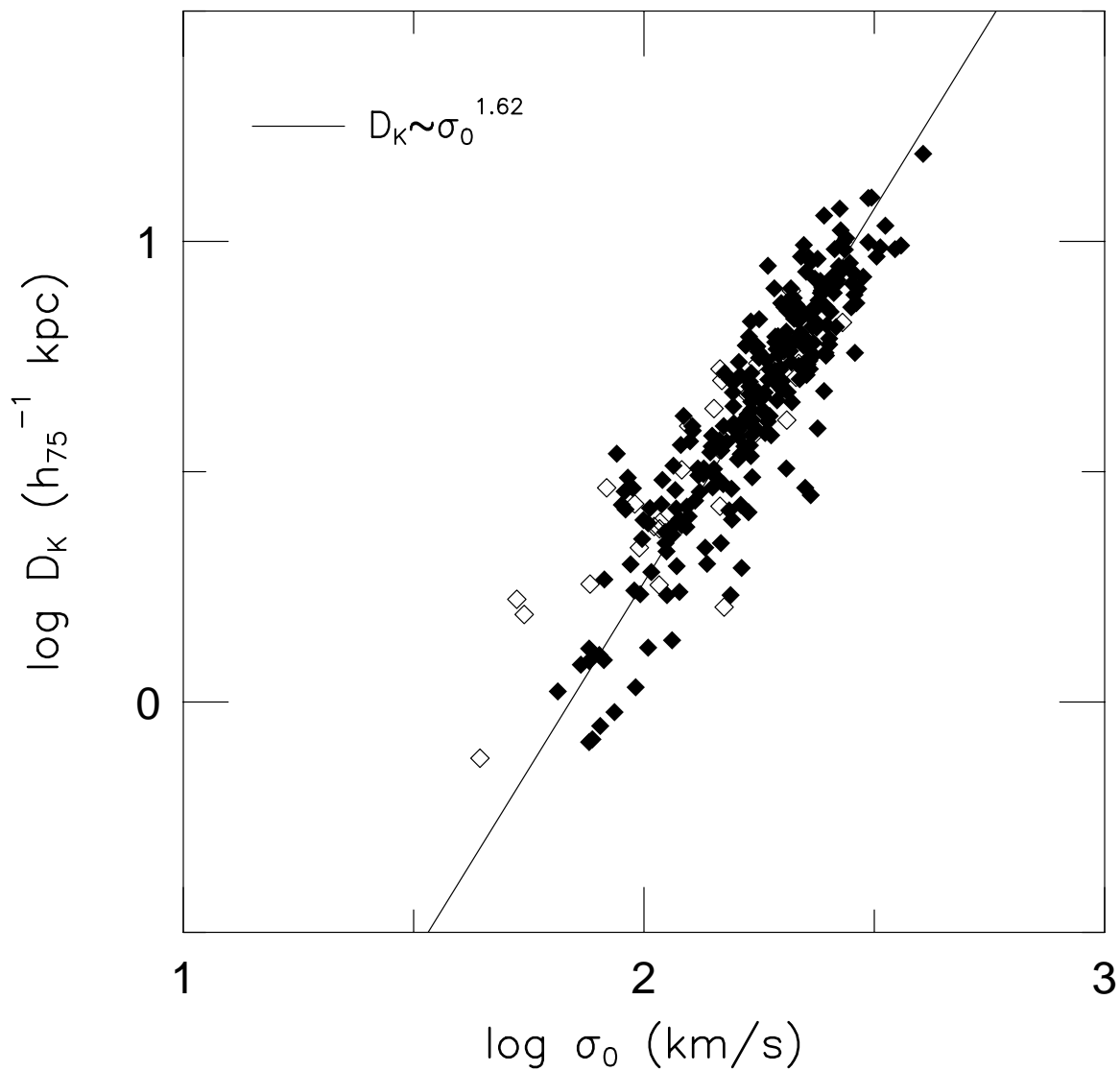


Fig. 3.— The D_K - σ_0 relation for the galaxies in the 16 clusters and groups of the survey, plotted in physical units. The scatter for this relation is 0.112 dex in $\log D_K$, which is slightly higher than the FP itself, since the D_K - σ_0 is not quite an edge-on view of the FP.

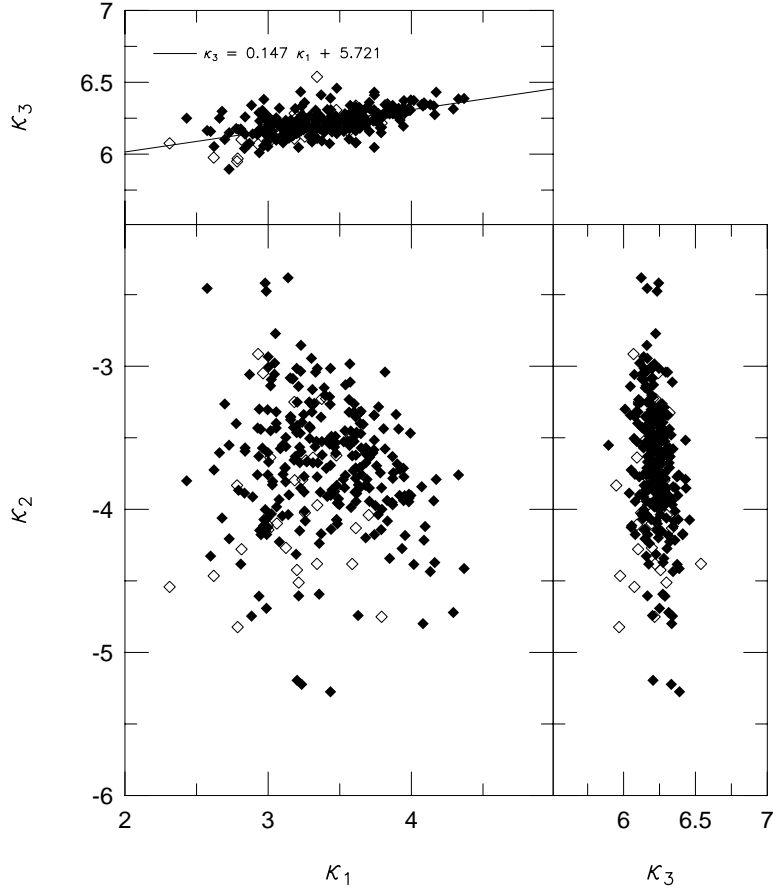


Fig. 4.— The K -band FP viewed in the κ -space perspective. This coordinate system (defined by Bender, Burstein, & Faber 1992) is given in Equation 5, and was designed such that κ_1 is roughly proportional to the logarithm of mass and κ_3 is roughly proportional to the logarithm of mass-to-light ratio. The fit in the top panel corresponds to the “observed” scaling relations $(M/L_K) \propto M^{0.15 \pm 0.01}$ or $(M/L_K) \propto L_K^{0.17 \pm 0.01}$, under the assumptions that there are no color gradients in elliptical galaxies and dynamical homology is preserved within the family of elliptical galaxies.

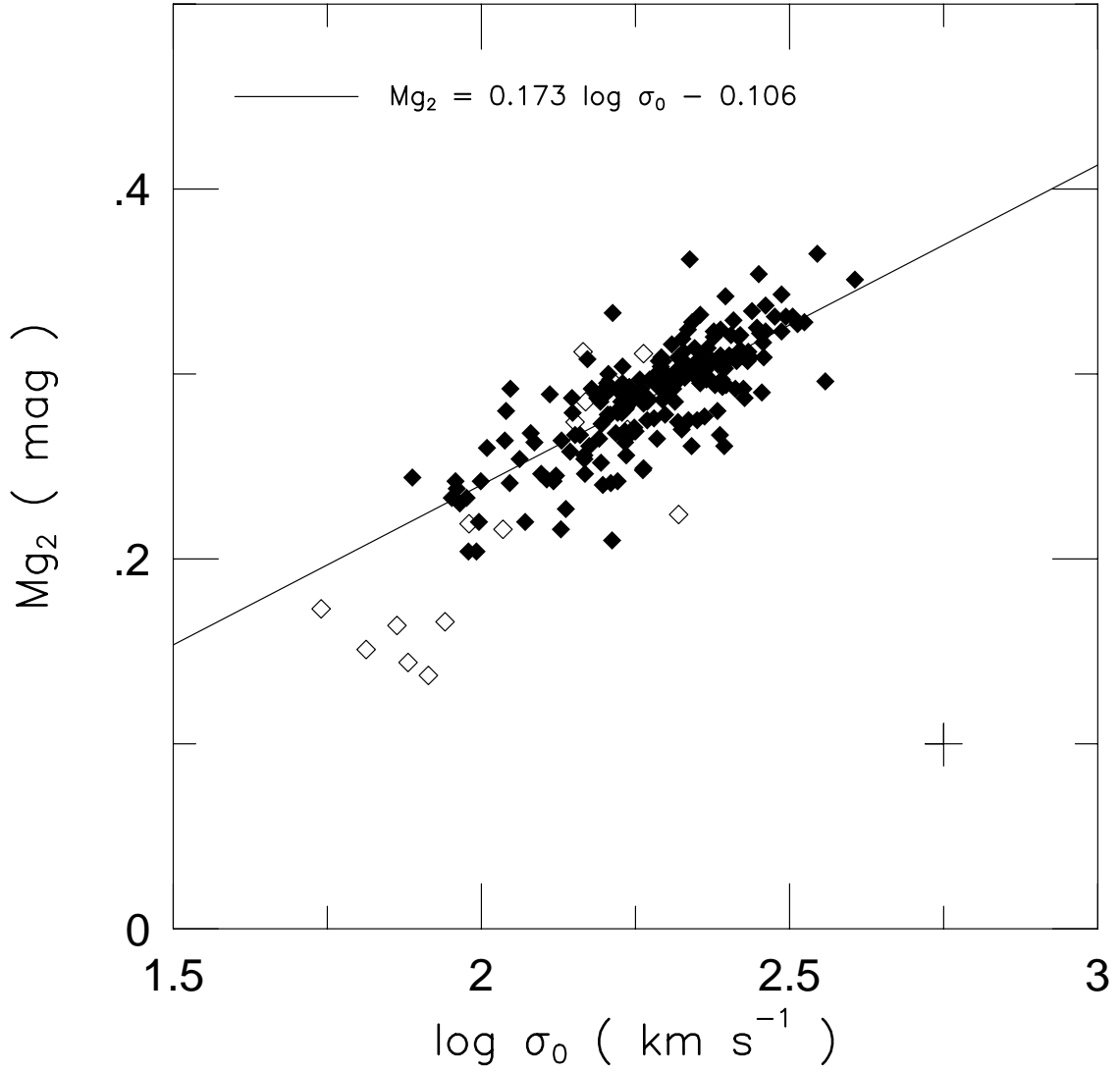


Fig. 5.— The Mg_2 – σ_0 relation for the 182 galaxies with Mg_2 measurements. The scatter about this relation is 0.019 mag in Mg_2 , which is significantly larger than the typical measurement uncertainties of 0.013 mag (shown in lower right-hand corner of figure).

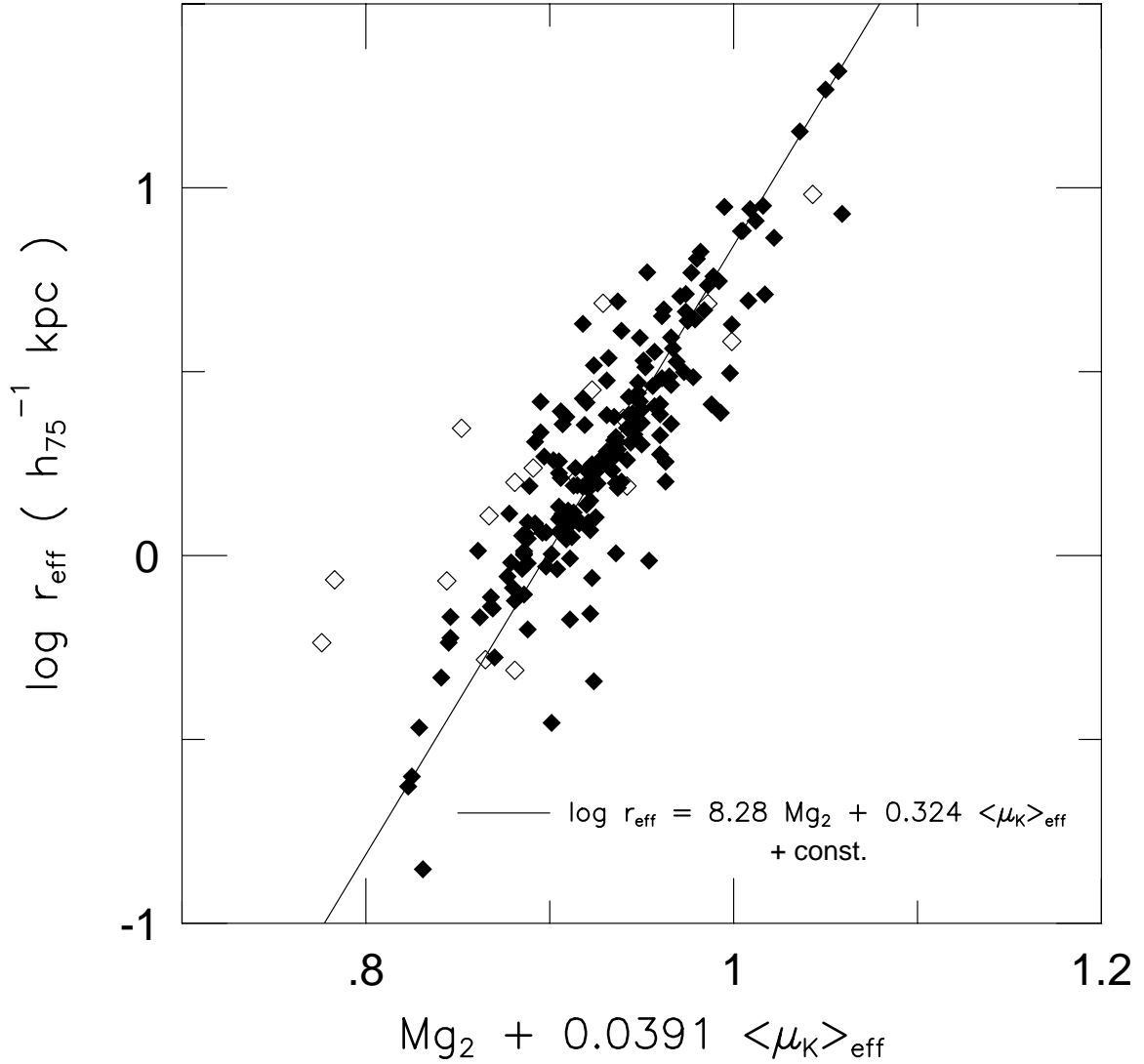


Fig. 6.— The near-infrared FP with the Mg_2 index substituted for the velocity dispersion. This figure is plotted to the same scale as Figure 2(a), hence a direct comparison of these two figures demonstrates how the scatter of the FP relation has increased by a factor of two by the substitution of Mg_2 for σ_0 . Only a small part of this increase in scatter can be attributed to the larger measurement uncertainties of Mg_2 compared to σ_0 , hence the correlation plotted in this figure cannot be an edge-on view of the FP.

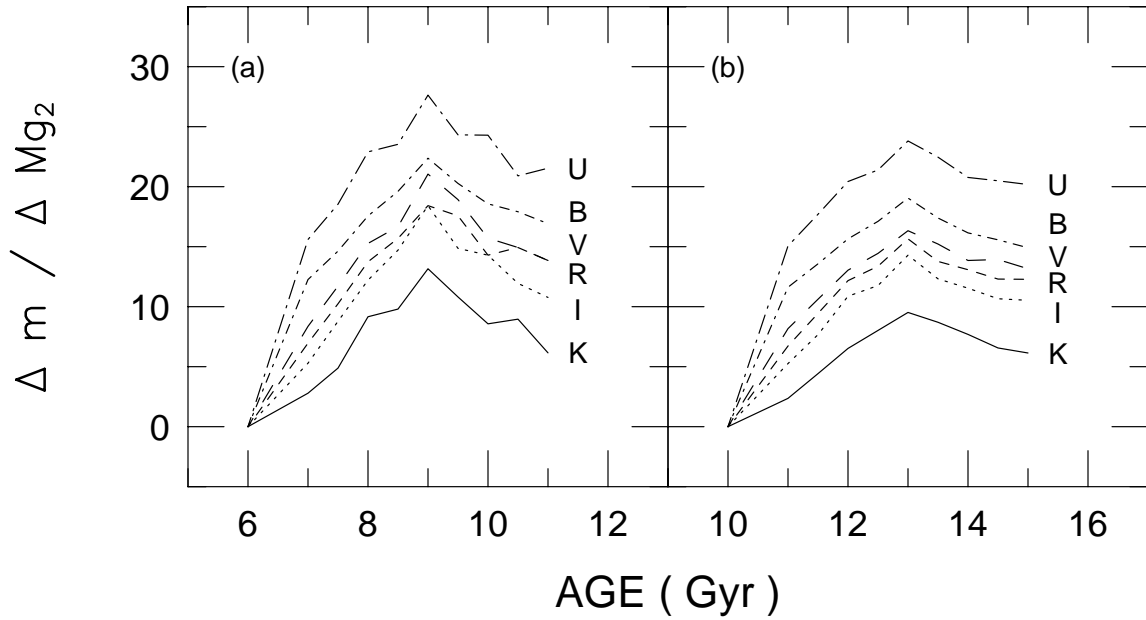


Fig. 7.— The ratio of the change in magnitude Δm to the change in the Mg_2 index for the *UBVRIK* bandpasses using the models of Worthey (1994). The two cases considered both have a 90% (by mass) old stellar population component of 11 Gyr (a) and 15 Gyr (b) and $[Fe/H]=0$ in addition to a 10% young stellar population that is 5 Gyr old at the present day.

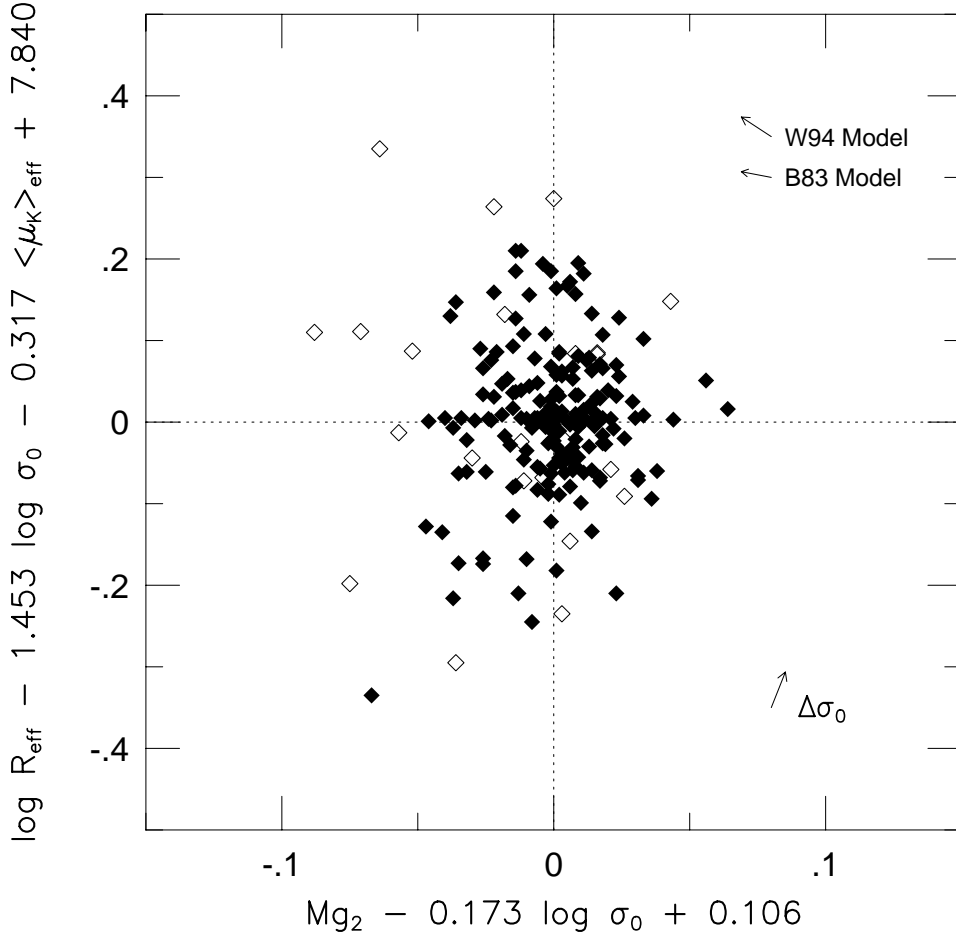


Fig. 8.— The residuals of the near-infrared FP plotted against the residuals of the Mg_2 - σ_0 relation. For the purpose of this comparison, only those galaxies with good Mg_2 measurements (see §3.4) were used to fit the near-infrared FP; the FP fit for these 182 galaxies is $r_{\text{eff}} \propto \sigma_0^{1.45} \langle \Sigma_K \rangle_{\text{eff}}^{-0.79}$. A correlation due to the measurement errors of $\log \sigma_0$ would act in the direction of the vectors in the lower-right of the panel labeled $\Delta\sigma_0$. If a galaxy had a starburst involving 10% of its mass at 5 Gyr before the present day, this would produce an offset as shown for the Bruzual (1983; B83) and Worthey (1994; W94) models. Since there is no such correlation along these model vectors between the two sets of residuals, this implies that there is no age effect, as traced by the Mg_2 - σ_0 relation, which is the sole cause of the intrinsic scatter of the near-infrared FP.

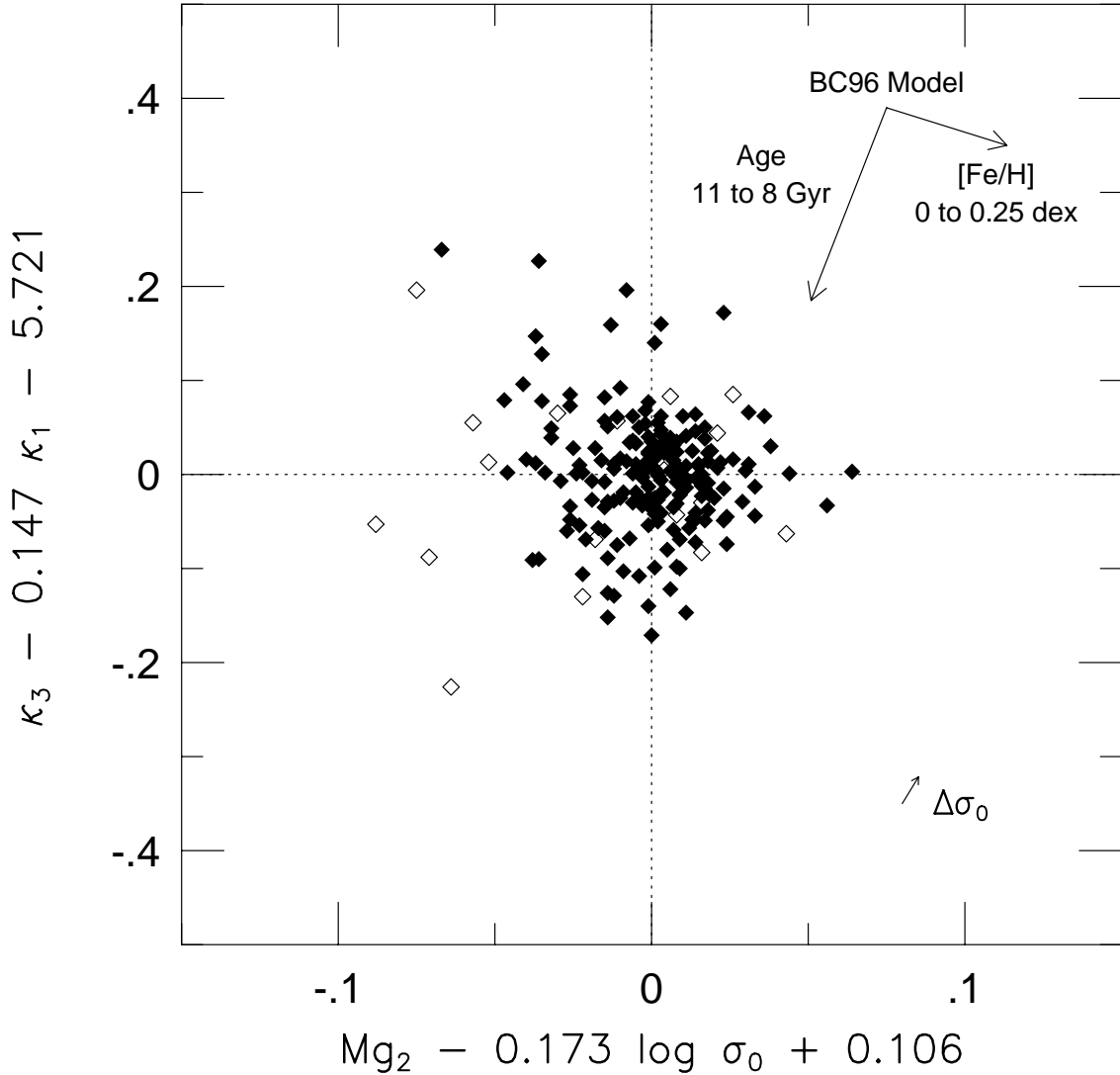


Fig. 9.— The residuals from the Mg_2 - σ_0 relation (Equation 10) plotted against the residuals from the κ_3 - κ_1 relation (Equation 6). Both relations show significant intrinsic scatter which could be due to variations in stellar populations at any given point on either relation. As shown by the vectors in the upper part of the figure, the Bruzual & Charlot (1996) models show that this diagram is a powerful diagnostic for separating the effects of age and metallicity. These models show the effect for changing the age from 11 to 8 Gyr for a solar metallicity population, and for changing $[Fe/H]$ from 0 to 0.25 dex in a 11 Gyr old population. The effect of correlated errors in σ_0 are shown in the lower-right of the figure. Variations in both age and metallicity at any given mass or luminosity appear to be necessary to explain the intrinsic scatter in this diagram and the lack of correlation along either vector in the upper right of the figure.

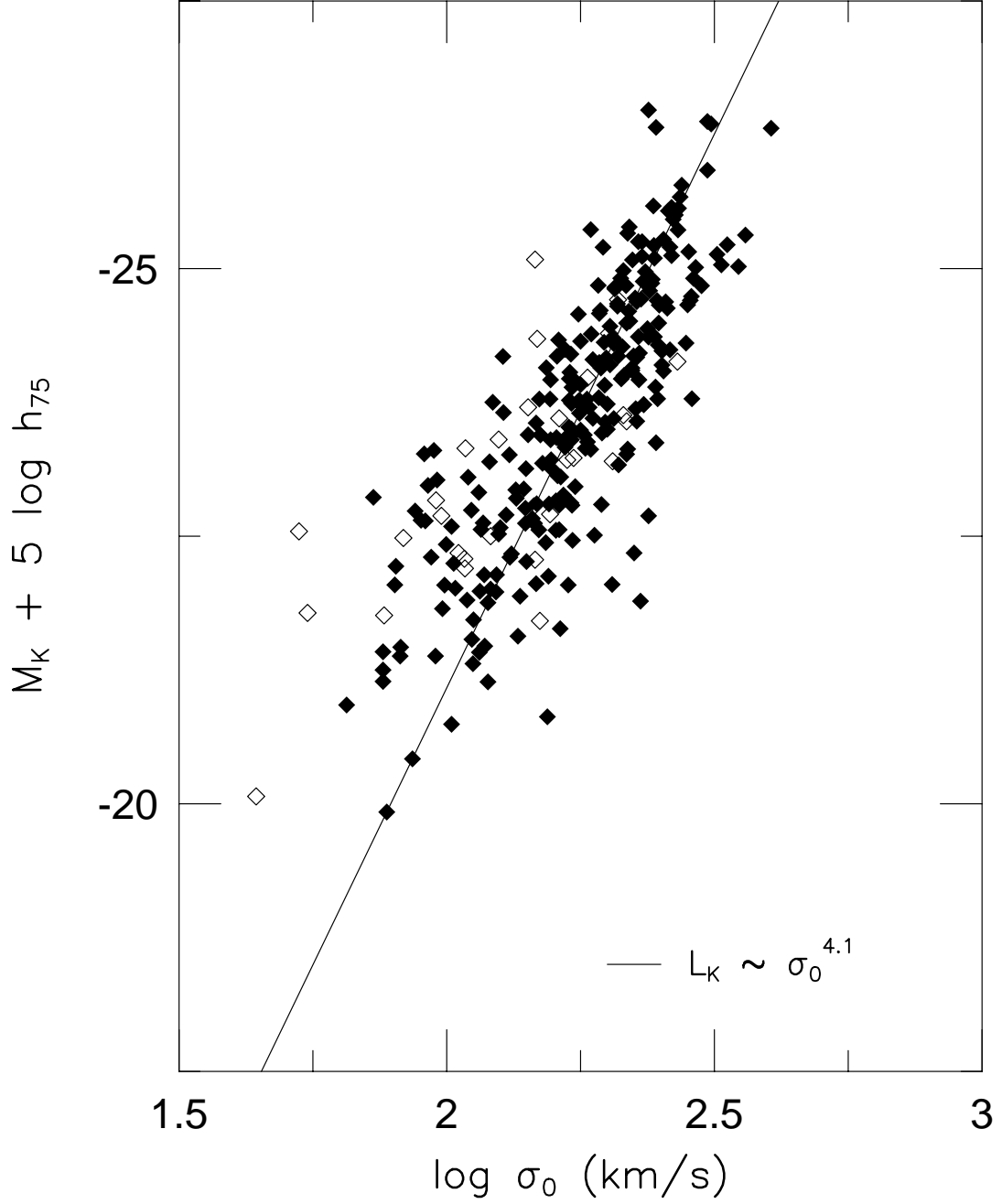


Fig. 10.— The Faber–Jackson relation between luminosity and central velocity dispersion. The best-fitting relation is $L_K \propto \sigma_0^{4.14 \pm 0.22}$ with a large scatter of 0.93 mag. The scatter is significantly smaller in the Coma cluster at 0.72 mag.

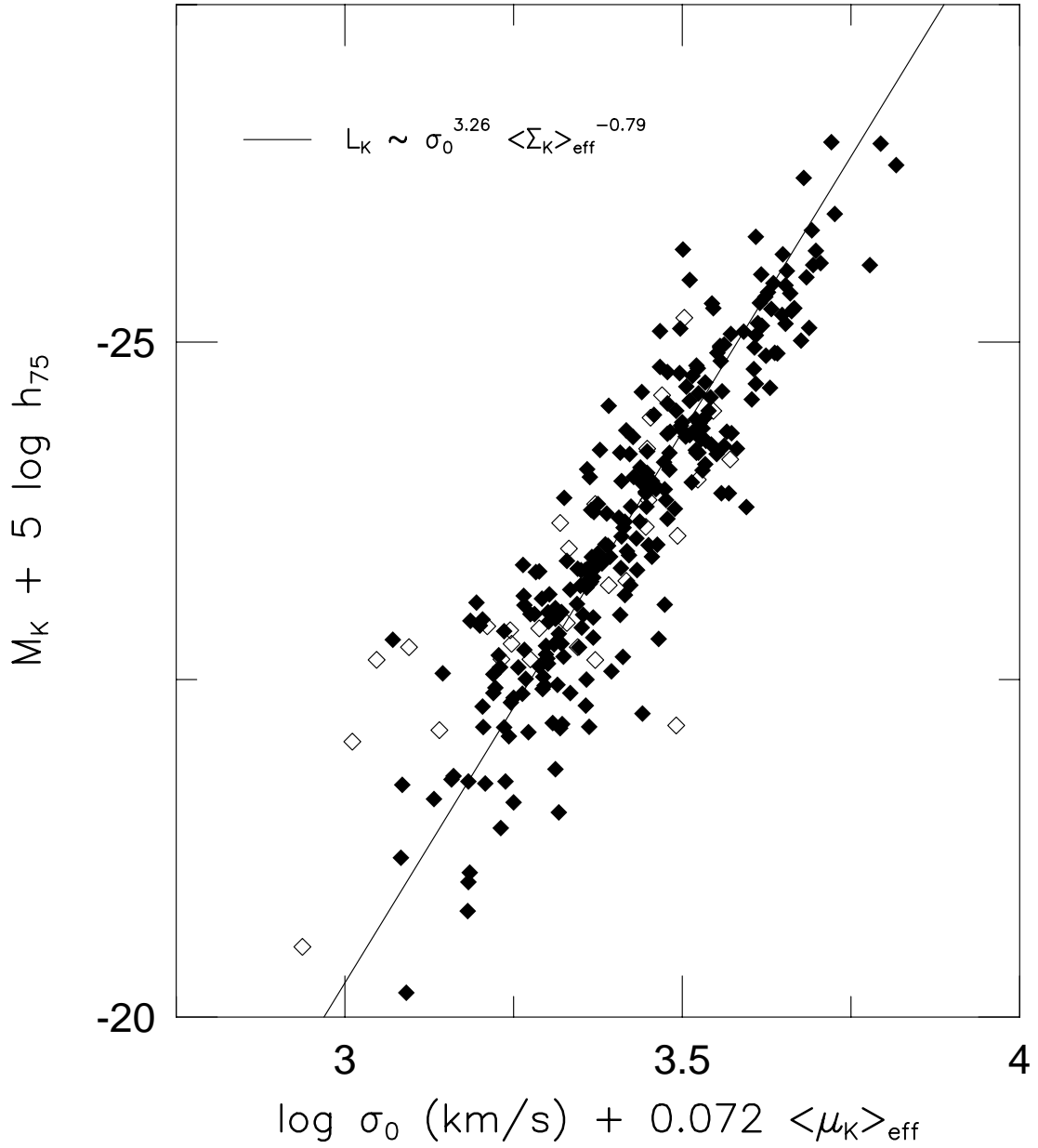


Fig. 11.— The “modified Faber–Jackson” form of the FP. The best–fitting relation is $L_K \propto \sigma_0^{3.26 \pm 0.19} \langle \Sigma_K \rangle_{\text{eff}}^{-0.59 \pm 0.06}$ with a scatter of 0.51 mag. This form of the FP is nearly identical to that of Figure 2 and Equation 2, although it shows 10% larger scatter primarily due to larger observational uncertainties.

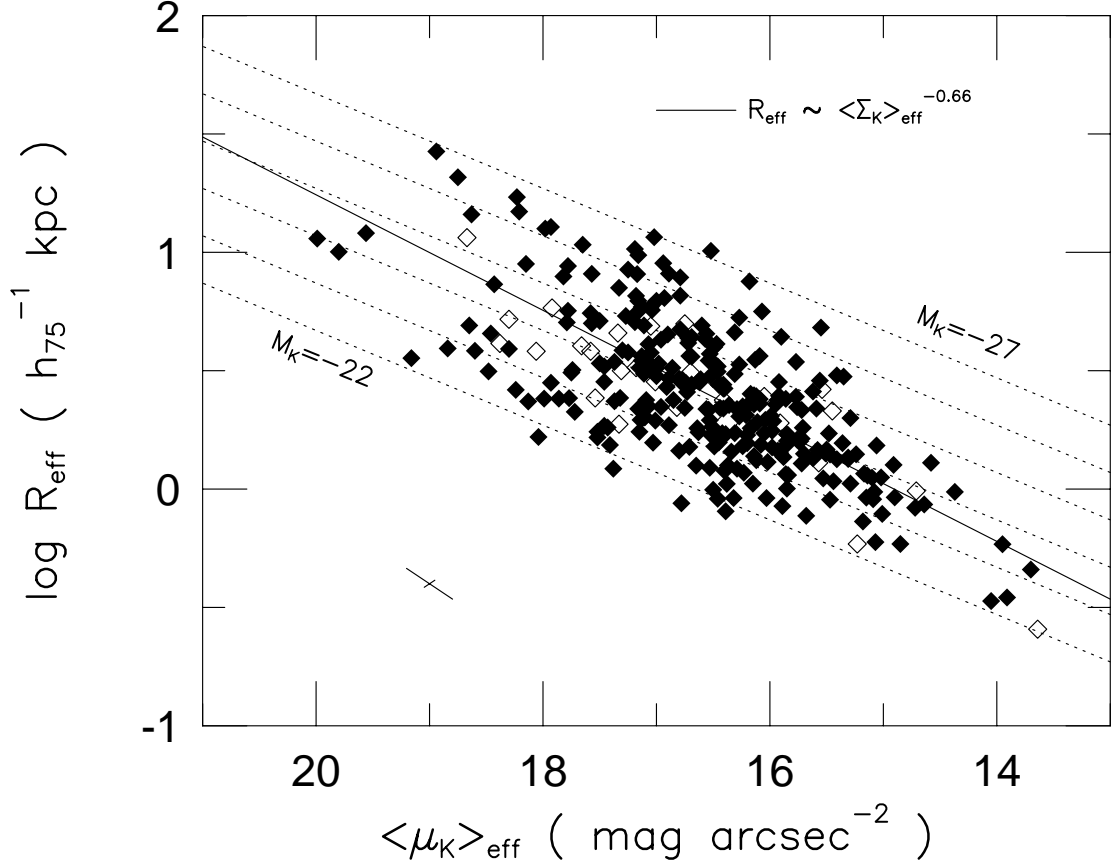


Fig. 12.— The Kormendy relation between effective radius and mean surface brightness. The best-fitting relation is $R_{\text{eff}} \propto \langle \mu_k \rangle_{\text{eff}}^{-0.61 \pm 0.07}$ with a scatter of 0.227 dex in $\log R_{\text{eff}}$, which is 2.4 times worse than the scatter of the FP (which has the additional σ_0 term). The scatter is significantly smaller in the Coma cluster at 0.198 dex. Measurement errors in R_{eff} and $\langle \mu \rangle_{\text{eff}}$ are correlated nearly along the relation, as shown by the representative error bars in the lower-left of the figure. The measurement uncertainties perpendicular to the relation are only 0.015 dex in $\log R_{\text{eff}} - 0.32 \langle \mu_K \rangle_{\text{eff}}$. Luminosity changes act perpendicular to the relation, and representative lines of $M_K = -22$ mag to $M_K = -27$ mag are shown as dotted lines.

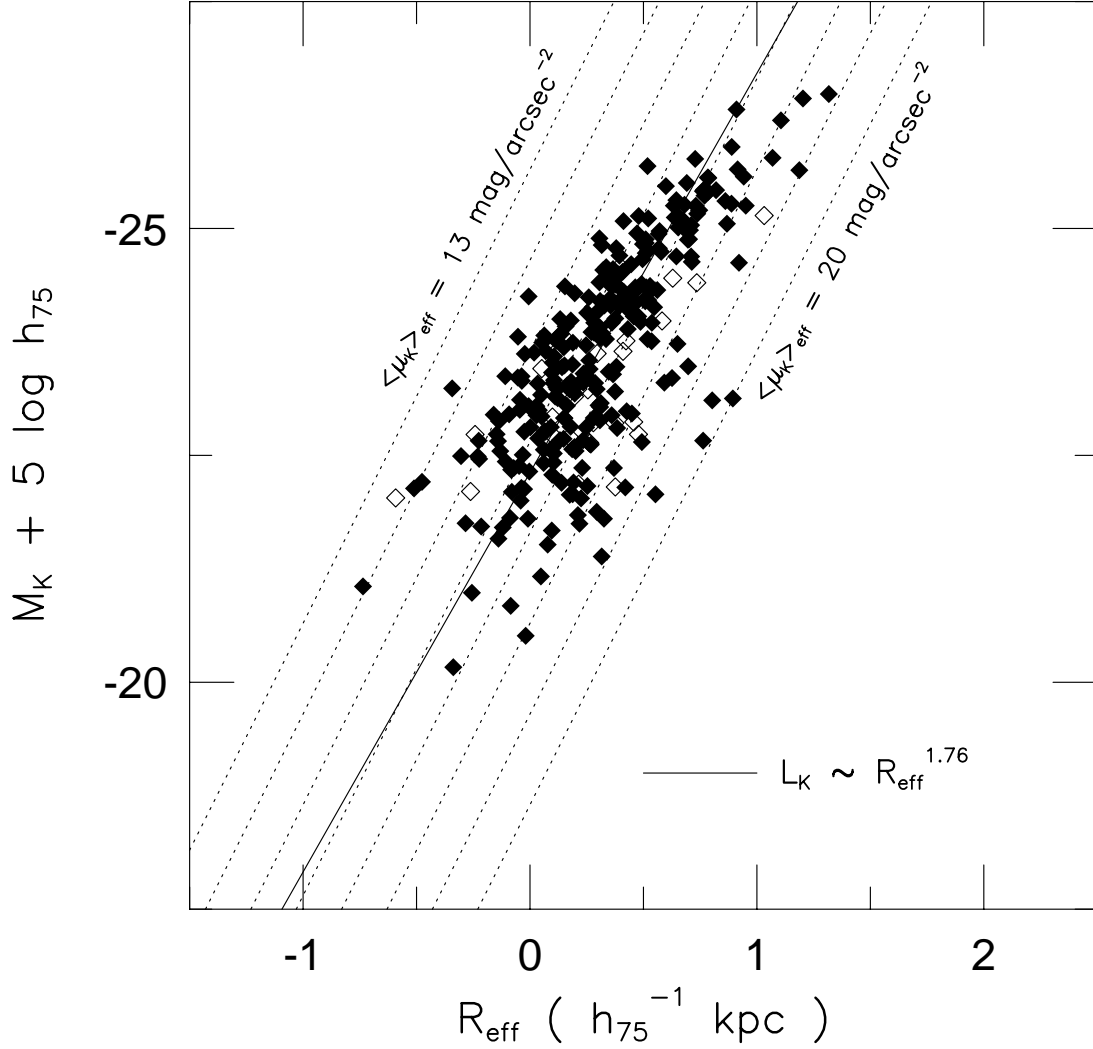


Fig. 13.— The relation between K -band total luminosity and effective radius given by $L_K \propto R_{\text{eff}}^{1.76 \pm 0.10}$. There is substantial intrinsic scatter in this relation due to variations in surface brightness. The dotted lines each represent the variation of M_K and R_{eff} at constant surface brightness.